AIMS Mathematics, 11(11): 36771–36805.
DOI: 10.3934/math.20261422
Received: 16 June 2026
Revised: 19 October 2026
Accepted: 30 October 2026
Published: 06 November 2026

https://www.aimspress.com/journal/Math

Research article

An individual-based mean-field network model for viral marketing diffusion

Angel Martin del Rey[1,*] **and Jose D. Hernandez Guillen**[2,]

[1] Department of Applied Mathematics, University of Salamanca, 37008-Salamanca, Spain

[2] Department of Mathematics, University of Extremadura, 06800-Mérida, Spain

* **Correspondence:** Email: delrey@usal.es.

Abstract: This paper presents a mathematical model for viral marketing diffusion on complex networks. The model considers four compartmental states: targets, who are initially unaware of the advertised product; spreading clients, who disseminate information and are customers of the product; spreading nonclients, who disseminate information without being customers; and inactive individuals, who are aware of the product but do not participate in its dissemination.

The proposed framework builds on established node-based mean-field approaches to spreading processes on complex networks. Specifically, deterministic equations are obtained through a first-order mean-field approximation to an interacting continuous-time stochastic process on the contact network. Consequently, the resulting node-level probabilities approximate the marginal state probabilities of the underlying stochastic process.

The distinguishing feature of the model is the explicit separation between spreading clients and spreading nonclients, allowing the diffusion of advertising information to be studied while retaining information about the customer status of the individuals involved.

The model incorporates the topology of the contact network and allows heterogeneous transition parameters. We analyze its diffusion dynamics, derive invasion thresholds for the network model and its homogeneous reduction, and investigate the accuracy of the mean-field approximation through comparisons with stochastic Monte Carlo simulations.

The proposed approach thus provides a marketing-oriented application of established network diffusion modeling techniques rather than a new general mathematical framework for individual-based spreading processes.

Keywords: viral marketing; mathematical model; mathematical epidemiology; individual-based model

Mathematics Subject Classification: 91-10, 90B60, 34D20

1. Introduction

In the digital age, viral marketing has emerged as a transformative force in shaping consumer behavior and brand outreach. Viral marketing refers to the strategic deployment of content that rapidly spreads across a wide audience, often propelled by users sharing and consuming the material. This phenomenon harnesses the power of social networks and online communities, considering the interconnected nature of individuals in the virtual space. The essence of viral marketing lies in its ability to reach a vast audience, creating a domino effect as people share compelling content using their social media profiles. The viral spread of information has redefined the traditional dynamics of communication and brand promotion, as online platforms serve as conduits (transmission vectors) for instantaneous and widespread dissemination. In our society, where digital connectivity is ubiquitous, viral marketing has become an integral aspect of modern advertising strategies, as it influences purchasing decisions and shapes public opinions. As businesses navigate the ever-evolving landscape of consumer engagement, understanding and harnessing the principles of viral marketing have become paramount, marking a paradigm shift in the way products and ideas are promoted in our interconnected and digitally-driven world.

A scientific comprehension of viral marketing has far-reaching implications for diverse fields, including commerce and trade, communication, and public health. In the first case, businesses can refine their marketing strategies, content creators can enhance engagement, and policymakers can leverage this knowledge to promote positive information cascades. In the realm of healthcare, viral marketing serves as a powerful catalyst for disseminating essential health information. Campaigns promoting public health initiatives, vaccination awareness, and disease prevention leverage the rapid spread of information through social networks. From a modeling perspective, these applications are particularly interesting because dissemination of a health message and adoption of the recommended behavior need not coincide, a distinction that is also central to the compartmental structure proposed in this work. In the field of communication, viral marketing revolutionizes the way information is shared and absorbed. Memes, videos, and interactive content disseminate rapidly, shaping societal conversations and influencing public opinion.

As a consequence, understanding the dynamics of viral marketing is crucial. The use of mathematical models to simulate and analyze the propagation of viral marketing provides a unique scientific perspective on this phenomenon. These models enable researchers to study the intricacies of how advertisement, products, or ideas proliferate through social networks. By capturing the underlying mechanisms driving viral marketing diffusion, we can gain insights into factors such as individual behavior, network structures, identificaton of key influencers, and the impact of various strategies on effective dissemination. Moreover, mathematical models offer a systematic approach to predict trends, to uncover patterns and principles governing the propagation process, and to dissect the complexities of viral dynamics.

Several mathematical approaches to modeling viral marketing diffusion have appeared in the scientific literature. One of the early works discussing the potential use of mathematical epidemiology in studying viral marketing spread is [1], where the authors developed a mathematical model that uses generation to track viral marketing transmission and time to determine the life of the campaign. Specifically, it is a susceptible-infectious-recovered (SIR) type model, where the branching process is determined by recurrence equations and involves three key coefficients: the contagion parameter,

the epidemic intensity, and the epidemic threshold parameter. Following this philosophy, in [2], the compartmental SIR model by Kermack-McKendrick is proposed as an example to illustrate the possible use of mathematical epidemiology to simulate viral marketing dissemination.

In [3], a spreading scheme was proposed based on some specific behaviors of users as the prompt action after activation (PAAA). The authors observed that the temporal differences between action and activation (to post a message) exhibit a heavy-tailed distribution. This is a continuation of the work in [4].

In [5], the authors studied the problem of incentive rate determination over a network of individuals with the aim to maximize the profit of a single good by a monopolist. This is done using an individual-based model, where the individuals are divided into three types: buyers, owners, and sellers, such that the dynamics is of the form buyer-owner-seller-buyer (BOSO).

Y. Ulyana and P. Andrij proposed in [6] a conceptual model for viral marketing spread based on the Monod equation, which defines a mathematical model for biomass growth.

In [7], the authors studied a SIR epidemiological model with application in marketing campaigns. Specifically, the mathematical properties of the model are analyzed from the parameters estimation and its sensitivity to the stability of the mathematical model. The same authors studied the optimal control strategies for a SIR viral marketing model in [8].

Of particular interest is the proposal by S. Bhattacharya *et al.* [9], where a global compartmental model was introduced. The population was divided into three major groups: unaware audience, broadcasters, and inerts. The dynamics of the process were described through the following system of ordinary differential equations (ODEs):

$$u'(t) = \mu - \rho\, b(t)\, u(t) - \mu\, u(t) \tag{1.1}$$

$$b'(t) = \rho\, b(t)\, u(t) - \sigma\, b(t) + \alpha\, b(t)\, i(t) - \mu\, b(t) \tag{1.2}$$

$$i'(t) = \sigma\, b(t) - \alpha\, b(t)\, i(t) - \mu\, i(t), \tag{1.3}$$

where $u(t)$, $b(t)$, and $i(t)$ represent the respective fractions of unaware individuals, broadcasters, and inerts. The parameters include ρ, representing the rate at which a broadcasting individual comes into contact with a potential audience member and shares the advertising message; σ, the rate at which spreading individuals stop advertising the product; α, the rate at which inerts return to advertising the product; and μ, the rate at which individuals appear and disappear from this advertising campaign (assuming a constant population).

Most of the compartmental models discussed above are formulated at the population level, with differential equations describing the evolution of compartment sizes or densities. Although such models provide useful information about the overall dynamics of viral marketing, they do not explicitly represent the contact structure of the population or the heterogeneity of individual interactions.

Network-based formulations offer a complementary approach by incorporating the underlying contact topology and allowing the evolution of node-level quantities to be studied. This motivates the consideration of individual-level network models for viral marketing diffusion.

Although many mathematical models of viral marketing are formulated at the population level, individual-based approaches have also been considered in this field, including the model proposed by Tavasoli et al. [5]. Moreover, individual-level approaches to spreading processes have been extensively investigated in the broader literature on mathematical epidemiology, information diffusion, and dynamical processes on complex networks. In particular, node-based mean-field models describe

the temporal evolution of marginal state probabilities associated with individual nodes while retaining information about the underlying contact network.

Such approaches have been developed and analyzed in several previous contributions, including the individual-level deterministic epidemic models studied by Sharkey [10] and the network mean-field formulation proposed by Van Mieghem et al. [11]. Consequently, the use of individual-state probabilities and network-dependent differential equations should be regarded as an established modeling methodology rather than as a novel feature of the present work.

Our objective is to adapt this methodology to a viral marketing mechanism in which individuals who disseminate information are distinguished according to whether or not they are clients of the advertised product.

The mathematical foundations of network-based spreading models are closely related to stochastic interacting particle systems and their deterministic approximations. In particular, the evolution equations for individual marginal probabilities generally involve joint probabilities of the states of neighboring nodes. The resulting hierarchy is not closed, and additional approximations are required to obtain a finite system of differential equations.

A standard first-order mean-field closure approximates these joint probabilities by products of the corresponding marginal probabilities. This approach has been extensively studied in the context of network epidemics, including node-based mean-field models and related moment-closure approximations. The limitations of such approximations are also well-known, particularly when correlations between neighboring nodes become significant. Moreover, the connection between epidemic invasion thresholds and spectral properties of network matrices has been established in previous studies. These results provide the mathematical background for the threshold analysis developed in the present paper.

A comprehensive account of epidemic processes on complex networks, including their mathematical formulations and threshold properties, can be found in the review by Pastor-Satorras et al. [12]. The application of epidemic-type mathematical models to the spreading of information and rumors also has a long history, dating back to the classical work of Daley and Kendall [13].

Our model should therefore be understood within this established mathematical framework, with its specific contribution lying in the formulation and analysis of a viral marketing process that distinguishes spreading clients from spreading nonclients.

In a node-based probabilistic formulation, each individual is associated with a vector whose components represent the probabilities of occupying the different states considered in the model. The resulting system of differential equations describes the temporal evolution of these probabilities while accounting for the contact network and the parameters governing the transitions between states.

Unlike population-level compartmental models, this approach retains information about individual nodes. However, the probability vector associated with a node does not determine its actual state with certainty. The expected compartment sizes can be approximated by summing the corresponding node-level probabilities, whereas assigning each node to its most probable state defines a separate classification procedure. This distinction is particularly important for the interpretation of the numerical results presented below.

In this work, we consider a four-state compartmental model for viral marketing diffusion on a contact network. The states correspond to individuals who are unaware of the advertised product (targets), spreading clients, spreading nonclients, and individuals who are aware of the product but do

not participate in its dissemination (inactive individuals).

Each node is characterized by a probability vector describing its possible states, and the evolution of these probabilities is modeled through a system of ordinary differential equations obtained under a first-order mean-field approximation. The formulation allows the characteristics of the contact network and the heterogeneity of the model parameters to be incorporated explicitly.

The contributions of the present work can be summarized as follows:

- First, we formulate a four-state network diffusion model specifically designed for viral marketing, distinguishing between spreading clients and spreading nonclients. This distinction allows the diffusion of advertising information to be modeled separately from the client status of the individuals participating in its dissemination.
- Second, we formulate a first-order node-based mean-field approximation for the proposed viral marketing process, in which the evolution of individual state probabilities depends on the contact network and on the corresponding transmission, branching, and deactivation parameters.
- Third, we analyze the invasion properties of the model. In particular, we derive the next-generation matrix for the network system and establish the corresponding reproduction number. We also investigate the homogeneous reduced system and clarify the relationship between its reproduction number and the spectral properties of the underlying network.
- Finally, we illustrate the diffusion dynamics through numerical experiments on complex networks and assess the accuracy of the mean-field approximation by comparison with stochastic Monte Carlo simulations.

These contributions extend established network-based mean-field modeling techniques to a specific viral marketing mechanism. We do not claim that the general mean-field methodology or the spectral approach to invasion thresholds is new.

The rest of the paper is organized as follows: In Section 2, the novel proposed model is described and analyzed. Some illustrative numerical simulations are shown in Section 3, and finally, conclusions and future work are introduced in Section 4.

2. Description and analysis of the proposed model

2.1. Preliminaries on complex network analysis

Let $\mathcal{G} = (\mathcal{V}, \mathcal{E})$ be a finite, simple, connected, undirected graph representing the social contact network, where $\mathcal{V} = \{v_1, v_2, \ldots, v_N\}$ is the set of nodes, and $\mathcal{E} \subseteq \{\{v_i, v_j\} : v_i, v_j \in V,\ i \neq j\}$ is the set of edges, with $|E| = M$. An edge $\{v_i, v_j\} \in E$ indicates that individuals i and j are socially connected and that information about the product can be transmitted between them.

The adjacency matrix associated with $\mathcal{G}$ is denoted by $A = (a_{ij})_{1\leq i,j\leq N}$, where

$$a_{ij} = \begin{cases} 1, & \text{if } \{v_i, v_j\} \in E, \\ 0, & \text{otherwise.} \end{cases} \tag{2.1}$$

Because the network is undirected, A is symmetric; that is, $A = A^\top$, and because self-loops are excluded, $a_{ii} = 0$ for every $i = 1, \ldots, N$.

The degree k_i of node $v_i \in \mathcal{V}$ is the number of nodes adjacent to v_i and is given by

$$k_i = \sum_{j=1}^{N} a_{ij}. \tag{2.2}$$

The mean degree of the network is therefore

$$\langle k \rangle = \frac{1}{N} \sum_{i=1}^{N} k_i = \frac{2M}{N}. \tag{2.3}$$

The density of the network is defined as

$$d_{\mathcal{G}} = \frac{2M}{N(N-1)}. \tag{2.4}$$

Consequently, $\langle k \rangle = (N-1)d_{\mathcal{G}}$.

A path between two nodes is a sequence of adjacent nodes joining them, and its length is the number of edges contained in the path. For two nodes $v_i, v_j \in \mathcal{V}$, the distance $d(v_i, v_j)$ is defined as the length of a shortest path joining them. Because $\mathcal{G}$ is connected and undirected, $d(v_i, v_j)$ is finite and symmetric.

The average path length is

$$L = \frac{2}{N(N-1)} \sum_{1 \le i < j \le N} d(v_i, v_j), \tag{2.5}$$

and the diameter is $D = \max\limits_{1 \le i,j \le N} d(v_i, v_j)$.

For a node v_i with $k_i \ge 2$, its local clustering coefficient is defined as

$$C_i = \frac{2E_i}{k_i(k_i-1)}, \tag{2.6}$$

where E_i denotes the number of edges between neighbors of v_i. For $k_i < 2$, we set $C_i = 0$. The mean clustering coefficient is

$$\overline{C} = \frac{1}{N} \sum_{i=1}^{N} C_i. \tag{2.7}$$

The degree distribution of the network, $P(k)$, can be defined as the probability distribution of degrees over the whole network, that is, $P(k) = N_k/N$, where N_k is the number of k-nodes. Complex networks can be classified in different types, depending mainly on the characteristics of the degree distribution.

Among the most frequently considered network classes are Erdös–Rényi random networks, small-world networks, and scale-free networks. Erdös–Rényi networks are characterized by independent edge formation with a prescribed probability. Small-world networks combine relatively short path lengths with substantial local clustering. Scale-free networks exhibit a heterogeneous degree distribution with a heavy tail so that a small number of highly connected nodes coexist with a large number of nodes of relatively low degree.

In the numerical experiments below, scale-free networks are generated using the Barabási–Albert (BA) preferential-attachment algorithm. Starting from an initial connected graph, each new node is

attached to m existing nodes, with attachment probabilities proportional to their current degrees. The resulting graph is undirected. For sufficiently large networks, its mean degree approaches $\langle k \rangle \simeq 2m$.

A (vertex) centrality associated to $\mathcal{G} = (\mathcal{V}, \mathcal{E})$ is a function $C : \mathcal{V} \to [0, 1]$ such that for every node $v \in \mathcal{V}$ and every graph isomorphism $\Phi \colon \mathcal{G} \to \mathcal{H}$, the following holds: $C(v) = C(\Phi(v))$; that is, C is a function invariant under isomorphisms. The objective of centrality measures (for nodes) is to quantify structural characteristics of nodes that determines its "importance" or "influence" within the network. Several centrality indices have been defined, but the most important are the following:

- The degree centrality of v_i is the average number of incident edges to such node; that is,

$$C_D(v_i) = \frac{k_i}{N-1}. \tag{2.8}$$

- The normalized closeness centrality of node v_i, which gives the mean distance from such node to the rest of nodes, is defined by

$$C_{\mathrm{CL}}(v_i) = \frac{N-1}{\sum\limits_{\substack{j=1 \\ j \neq i}}^{N} d(v_i, v_j)}. \tag{2.9}$$

- Betweenness centrality of the node $v_i \in \mathcal{V}$ is given by the relative number of shortest paths between two nodes that run through the node considered:

$$C_B(v_i) = \frac{2}{(N-1)(N-2)} \sum_{\substack{1 \leq r < s \leq N \\ r \neq i, s \neq i}} \frac{l_{rs}(v_i)}{\ell_{rs}}, \tag{2.10}$$

  where ℓ_{rs} is the total number of geodesic paths from v_r to v_s, and $l_{rs}(v_i)$ stands for the number of such paths that pass through the node v_i.
- The eccentricity centrality of the node v_i is defined as follows:

$$C_E(v_i) = \frac{1}{\max\{d\left(v_i, v_j\right),\ j \neq i,\ 1 \leq j \leq N\}}. \tag{2.11}$$

2.2. Model overview

As is mentioned above, the proposed model to simulate the dynamics of a viral marketing campaign is compartmental and individual in nature, where the states of each individual over continuous time are defined by a vector of probabilities. Specifically, it is a compartmental model because the population is divided into four compartments: the target population (T), consisting of individuals who are unaware of the product (and, obviously, are not customers) and are the focus of the campaign; the spreading clients (S_c), who are individuals on whom the campaign has been entirely successful, being both consumers of the product and advocates who spread its awareness; the spreading nonclients (S_n), encompassing individuals who, after receiving the advertisement, decide not to purchase the product (for various reasons) but still contribute to its promotion (this group may include professionals hired by the brand for product promotion); and finally, the compartment of inert or nonspreading individuals (I), comprising all individuals, consumers or nonconsumers, who do not participate in the diffusion process.

Moreover, as mentioned, it is a model of individual nature because the goal is to study the evolution of the specific state (target, spreading client, spreading nonclient, or nonspreader) of each individual over continuous time. In this way, we will denote by

$$\text{state}[i,t] = (T_i(t), S_{c,i}(t), S_{n,i}(t), I_i(t)) \in [0,1] \times [0,1] \times [0,1] \times [0,1] \tag{2.12}$$

the state of the ith individual at time t, where $T_i(t)$ represents the probability of being a target audience at time t; $S_{c,i}(t)$ denotes the probability of being a spreading client at t; $S_{n,i}(t)$ is the probability of being a nonclient spreader at t; and finally, $I_i(t) = 1 - T_i(t) - S_{c,i}(t) - S_{n,i}(t)$ is the probability of being an individual who does not advertise the article at time t.

These probabilities will change over time according to a "transition rule" described by a system of ordinary differential equations in which the variables are the probabilities themselves. The following coefficients are taken into account for each individual (see Figure 1):

- Attention rate, $\rho_i \geq 0$: Represents the rate at which the advertising campaign reaches the ith target individual through spreading neighbors. Therefore, ρ_i has units of inverse time.
- Diffusion branching probabilities, $\delta_{c,i}$ and $\delta_{n,i}$: Represent the probabilities that upon exposure to the campaign, the ith target individual becomes, respectively, a spreading client or a spreading nonclient. Therefore, these parameters are dimensionless and satisfy the following:

$$\delta_{c,i} \geq 0, \quad \delta_{n,i} \geq 0, \quad \delta_{c,i} + \delta_{n,i} \leq 1. \tag{2.13}$$

  The complementary probability $1 - \delta_{c,i} - \delta_{n,i}$ corresponds to a direct transition from the target state to the inert state.
- Deactivation rates, $\sigma_{c,i} \geq 0$ and $\sigma_{n,i} \geq 0$: Represent the rates at which a spreading client or a spreading nonclient, respectively, becomes inactive with respect to the advertising campaign. These parameters have units of inverse time.

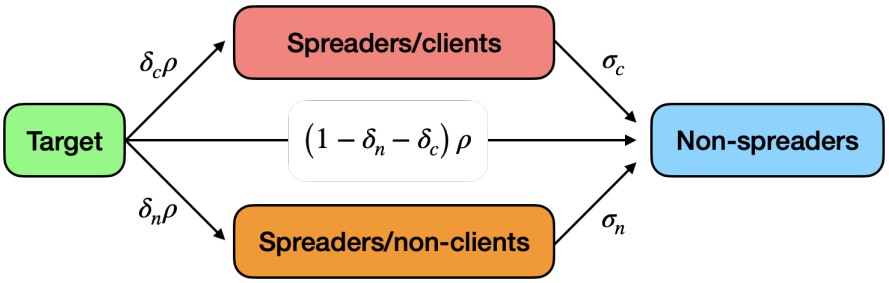


Figure 1. Flow diagram associated to the compartmental model.

Although the proposed framework is inspired by mathematical epidemiology, the analogy between infectious-disease transmission and information diffusion should not be interpreted literally. Biological transmission is mainly governed by physical contact and pathogen-related mechanisms, whereas the decision to pay attention to, share, or stop sharing marketing information may depend on individual preferences, previous experiences, perceived credibility, social influence, and other behavioral factors. In the present model, such individual heterogeneity can be partially represented through the node-dependent parameters ρ_i, $\delta_{c,i}$, $\delta_{n,i}$, $\sigma_{c,i}$, and $\sigma_{n,i}$. Moreover, simultaneous exposure to several spreading

neighbors is incorporated through the network interaction term, as the diffusion pressure acting on an individual increases with the number of neighboring spreaders. However, the current formulation is memoryless and assumes additive contributions from spreading neighbors. Consequently, it does not explicitly account for cumulative effects of previous exposures, saturation or advertising fatigue, reinforcement mechanisms, or behavioral changes induced by repeated exposure. Incorporating these effects would require, for example, history-dependent transition rates, nonlinear exposure functions, or additional behavioral states. These extensions constitute an interesting direction for future developments of the model.

2.3. Mathematical description and analysis of the proposed model

As described in Subsection 2.1, the social contact topology is represented by a simple, connected, undirected graph $\mathcal{G} = (\mathcal{V}, \mathcal{E})$. An edge $\{v_i, v_j\} \in E$ indicates that individuals i and j are socially connected and that information about the product may be transmitted between them. Therefore, the adjacency matrix is symmetric, that is; $a_{ij} = a_{ji}$.

For the ith node, the total spreading pressure generated by its neighbors is represented by

$$\sum_{j=1}^{N} a_{ij} \left(S_{c,j}(t) + S_{n,j}(t) \right). \tag{2.14}$$

Thus, only individuals adjacent to node i contribute to its instantaneous diffusion pressure.

As mentioned earlier, the dynamics governing the evolution of the probability vectors,

$$\text{state}[i, t] = \left(T_i(t), S_{c,i}(t), S_{n,i}(t), I_i(t) \right), \tag{2.15}$$

with $1 \leq i \leq N$, are described by a system of differential equations as follows:

$$\begin{aligned}
T_i'(t) &= -\rho_i T_i(t) \sum_{1 \leq j \leq N} a_{ij} \left(S_{c,j}(t) + S_{n,j}(t) \right), && (2.16)\\
S_{c,i}'(t) &= \delta_{c,i} \rho_i T_i(t) \sum_{1 \leq j \leq N} a_{ij} \left(S_{c,j}(t) + S_{n,j}(t) \right) - \sigma_{c,i} S_{c,i}(t) && (2.17)\\
S_{n,i}'(t) &= \delta_{n,i} \rho_i T_i(t) \sum_{1 \leq j \leq N} a_{ij} \left(S_{c,j}(t) + S_{n,j}(t) \right) - \sigma_{n,i} S_{n,i}(t), && (2.18)\\
I_i'(t) &= (1 - \delta_{n,i} - \delta_{c,i}) \rho_i T_i(t) \sum_{1 \leq j \leq N} a_{ij} \left(S_{c,j}(t) + S_{n,j}(t) \right) + \sigma_{c,i} S_{c,i}(t) + \sigma_{n,i} S_{n,i}(t). && (2.19)
\end{aligned}$$

For the probabilistic interpretation of the model, we assume throughout that for every $i = 1, \ldots, N$,

$$\rho_i \geq 0, \quad \sigma_{c,i} \geq 0, \quad \sigma_{n,i} \geq 0, \quad \delta_{c,i} \geq 0, \quad \delta_{n,i} \geq 0, \quad \delta_{c,i} + \delta_{n,i} \leq 1. \tag{2.20}$$

Moreover, the initial state of every node is assumed to satisfy $T_i(0), S_{c,i}(0), S_{n,i}(0), I_i(0) \geq 0$, and

$$T_i(0) + S_{c,i}(0) + S_{n,i}(0) + I_i(0) = 1. \tag{2.21}$$

For each node i, set

$$\Delta_i = \left\{ (T_i, S_{c,i}, S_{n,i}, I_i) \in \mathbb{R}^4_{\geq 0} : T_i + S_{c,i} + S_{n,i} + I_i = 1 \right\}, \tag{2.22}$$

and define the state space of the full network model by $\Omega = \Delta_1 \times \ldots \times \Delta_N$.

Proposition 1 (Well-posedness and positive invariance)**.** *Under the parameter assumptions stated above, for every initial condition in* Ω*, the system* (2.16)–(2.19) *admits a unique solution defined for all* $t \geq 0$*. Moreover,* Ω *is positively invariant. Consequently, for every* $i = 1, \ldots, N$ *and every* $t \geq 0$*,*

$$T_i(t), S_{c,i}(t), S_{n,i}(t), I_i(t) \in [0, 1], \tag{2.23}$$

and $T_i(t) + S_{c,i}(t) + S_{n,i}(t) + I_i(t) = 1$*. Hence, the four state variables retain their probabilistic interpretation for all* $t \geq 0$*.*

Proof. For convenience, define

$$\Lambda_i(t) = \rho_i \sum_{j=1}^{N} a_{ij} \left(S_{c,j}(t) + S_{n,j}(t) \right). \tag{2.24}$$

Because the adjacency matrix is non-negative, and $\rho_i \geq 0$, we have $\Lambda_i(t) \geq 0$ whenever the state variables are non-negative. The equations for node i can then be written as follows:

$$\begin{aligned} T_i' &= -T_i \Lambda_i, && (2.25)\\ S_{c,i}' &= \delta_{c,i} T_i \Lambda_i - \sigma_{c,i} S_{c,i}, && (2.26)\\ S_{n,i}' &= \delta_{n,i} T_i \Lambda_i - \sigma_{n,i} S_{n,i}, && (2.27)\\ I_i' &= (1 - \delta_{c,i} - \delta_{n,i}) T_i \Lambda_i + \sigma_{c,i} S_{c,i} + \sigma_{n,i} S_{n,i}. && (2.28) \end{aligned}$$

We first verify nonnegativity:

- On the boundary $T_i = 0$, it is $T_i' = 0$.
- On the boundary $S_{c,i} = 0$, it is $S_{c,i}' = \delta_{c,i} T_i \Lambda_i \geq 0$.
- On the boundary $S_{n,i} = 0$, we have $S_{n,i}' = \delta_{n,i} T_i \Lambda_i \geq 0$.
- Finally, on the boundary $I_i = 0$,

$$I_i' = (1 - \delta_{c,i} - \delta_{n,i}) T_i \Lambda_i + \sigma_{c,i} S_{c,i} + \sigma_{n,i} S_{n,i} \geq 0, \tag{2.29}$$

  where the inequality follows from $\delta_{c,i} + \delta_{n,i} \leq 1$ and the nonnegativity of all parameters and state variables.

Thus, the vector field points inward or is tangent to the nonnegative orthant on each boundary face, and nonnegative initial data remain nonnegative.

Furthermore, summing the four equations corresponding to the ith node gives

$$\frac{d}{dt} \left(T_i + S_{c,i} + S_{n,i} + I_i \right) = 0, \tag{2.30}$$

and therefore,

$$T_i(t) + S_{c,i}(t) + S_{n,i}(t) + I_i(t) = T_i(0) + S_{c,i}(0) + S_{n,i}(0) + I_i(0) = 1 \tag{2.31}$$

for every $t \geq 0$. Hence, each Δ_i is positively invariant, and consequently, so is $\Omega = \Delta_1 \times \ldots \times \Delta_N$.

Finally, the right-hand side of the system is polynomial in the state variables and is therefore locally Lipschitz continuous. Thus, a unique local solution exists for every initial condition. Because Ω is compact and positively invariant, the solution remains bounded and can be extended for all $t \geq 0$. □

As a consequence of this result, the fourth state variable satisfies

$$I_i(t) = 1 - T_i(t) - S_{c,i}(t) - S_{n,i}(t) \tag{2.32}$$

for every $t \geq 0$. As a consequence, the full system (2.16)–(2.19) can be equivalently reduced to the following $3N$-dimensional system:

$$\begin{aligned}
T_i'(t) &= -\rho_i T_i(t) \sum_{1\leq j\leq N} a_{ij}\left(S_{c,j}(t) + S_{n,j}(t)\right), && (2.33)\\
S_{c,i}'(t) &= \delta_{c,i}\rho_i T_i(t) \sum_{1\leq j\leq N} a_{ij}\left(S_{c,j}(t) + S_{n,j}(t)\right) - \sigma_{c,i} S_{c,i}(t) && (2.34)\\
S_{n,i}'(t) &= \delta_{n,i}\rho_i T_i(t) \sum_{1\leq j\leq N} a_{ij}\left(S_{c,j}(t) + S_{n,j}(t)\right) - \sigma_{n,i} S_{n,i}(t). && (2.35)
\end{aligned}$$

Additionally, using matrix notation, the system can be written as follows:

$$\begin{aligned}
T'(t) &= -\rho \operatorname{diag}(T(t))\, A\,(S_c(t) + S_n(t)), && (2.36)\\
S_c'(t) &= \delta_c \rho \operatorname{diag}(T(t))\, A\,(S_c(t) + S_n(t)) - \sigma_c S_c(t), && (2.37)\\
S_n'(t) &= \delta_n \rho \operatorname{diag}(T(t))\, A\,(S_c(t) + S_n(t)) - \sigma_n S_n(t), && (2.38)
\end{aligned}$$

where

$$\begin{aligned}
T(t) &= (T_1(t), \ldots, T_N(t))^{\intercal}, && (2.39)\\
S_c(t) &= (S_{c,1}(t), \ldots, S_{c,N}(t))^{\intercal}, && (2.40)\\
S_n(t) &= (S_{n,1}(t), \ldots, S_{n,N}(t))^{\intercal}, && (2.41)\\
\rho &= \operatorname{diag}(\rho_1, \ldots, \rho_N) = \begin{pmatrix} \rho_1 & 0 & \ldots & 0 \\ 0 & \rho_2 & \ddots & \vdots \\ \vdots & \ddots & \ddots & 0 \\ 0 & \ldots & 0 & \rho_N \end{pmatrix}, && (2.42)\\
\delta_c &= \operatorname{diag}(\delta_{c,1}, \ldots, \delta_{c,N}), && (2.43)\\
\delta_n &= \operatorname{diag}(\delta_{n,1}, \ldots, \delta_{n,N}), && (2.44)\\
\sigma_c &= \operatorname{diag}(\sigma_{c,1}, \ldots, \sigma_{c,N}), && (2.45)\\
\sigma_n &= \operatorname{diag}(\sigma_{n,1}, \ldots, \sigma_{n,N}). && (2.46)
\end{aligned}$$

Note that all parameter matrices $\rho, \delta_c, \delta_n, \sigma_c$, and σ_n are diagonal matrices of order N. In particular, the deactivation terms are expressed as

$$\sigma_c S_c(t) = \begin{pmatrix} \sigma_{c,1} S_{c,1}(t) \\ \sigma_{c,2} S_{c,2}(t) \\ \vdots \\ \sigma_{c,N} S_{c,N}(t) \end{pmatrix}, \quad \sigma_n S_n(t) = \begin{pmatrix} \sigma_{n,1} S_{n,1}(t) \\ \sigma_{n,2} S_{n,2}(t) \\ \vdots \\ \sigma_{n,N} S_{n,N}(t) \end{pmatrix}. \tag{2.47}$$

Consequently, the matrix formulation is dimensionally consistent and is equivalent, component by component, to the original system of differential equations.

2.4. Invasion threshold for the network model

We first derive an invasion threshold for the full network model before considering its homogeneous, well-mixed reduction. Let $E^* = (T^*, 0, 0, I^*)$ be a diffusion-free equilibrium, where $T^* = (T_1^*, \dots, T_N^*)^\top$.

Define

$$B^* = \operatorname{diag}(\rho_1 T_1^*, \dots, \rho_N T_N^*)\, A. \tag{2.48}$$

The linearization of the spreading subsystem around E^* gives

$$\frac{d}{dt}\begin{pmatrix}\mathbf{S}_c\\ \mathbf{S}_n\end{pmatrix} = \left[\begin{pmatrix}\boldsymbol{\delta}_c B^* & \boldsymbol{\delta}_c B^*\\ \boldsymbol{\delta}_n B^* & \boldsymbol{\delta}_n B^*\end{pmatrix} - \begin{pmatrix}\boldsymbol{\sigma}_c & 0\\ 0 & \boldsymbol{\sigma}_n\end{pmatrix}\right]\begin{pmatrix}\mathbf{S}_c\\ \mathbf{S}_n\end{pmatrix}, \tag{2.49}$$

and the corresponding next-generation matrix is therefore

$$K = \begin{pmatrix}\boldsymbol{\delta}_c B^* \boldsymbol{\sigma}_c^{-1} & \boldsymbol{\delta}_c B^* \boldsymbol{\sigma}_n^{-1}\\ \boldsymbol{\delta}_n B^* \boldsymbol{\sigma}_c^{-1} & \boldsymbol{\delta}_n B^* \boldsymbol{\sigma}_n^{-1}\end{pmatrix}. \tag{2.50}$$

Proposition 2 (Network invasion threshold)**.** *The local invasion threshold associated with the diffusion-free equilibrium E^* is*

$$\mathcal{R}_{\text{net}}(T^*) = \varrho(K), \tag{2.51}$$

where $\varrho(\cdot)$ denotes the spectral radius. Moreover,

$$\mathcal{R}_{\text{net}}(T^*) = \varrho(K) = \varrho\left[\left(\boldsymbol{\sigma}_c^{-1}\boldsymbol{\delta}_c + \boldsymbol{\sigma}_n^{-1}\boldsymbol{\delta}_n\right) B^*\right]. \tag{2.52}$$

If $\mathcal{R}_{\text{net}}(T^*) < 1$, sufficiently small spreading perturbations decay locally in the directions transverse to the diffusion-free equilibrium manifold, whereas $\mathcal{R}_{\text{net}}(T^*) > 1$ implies linear instability in a spreading direction.

Proof. Let

$$\mathcal{F} = \begin{pmatrix}\boldsymbol{\delta_c} B^* & \boldsymbol{\delta_c} B^*\\ \boldsymbol{\delta_n} B^* & \boldsymbol{\delta_n} B^*\end{pmatrix}, \qquad \mathcal{V} = \begin{pmatrix}\boldsymbol{\sigma_c} & 0\\ 0 & \boldsymbol{\sigma_n}\end{pmatrix}. \tag{2.53}$$

Then, the next-generation matrix is $K = \mathcal{F}\mathcal{V}^{-1}$.

Writing

$$X = \begin{pmatrix}\boldsymbol{\delta_c} B^*\\ \boldsymbol{\delta_n} B^*\end{pmatrix}, \qquad Y = \begin{pmatrix}\boldsymbol{\sigma_c}^{-1} & \boldsymbol{\sigma_n}^{-1}\end{pmatrix}, \tag{2.54}$$

we have $K = XY$. As the nonzero eigenvalues of XY and YX coincide,

$$\varrho(K) = \varrho(YX) = \varrho\left[\boldsymbol{\sigma_c}^{-1}\boldsymbol{\delta_c} B^* + \boldsymbol{\sigma_n}^{-1}\boldsymbol{\delta_n} B^*\right], \tag{2.55}$$

and therefore,

$$\mathcal{R}_{\text{net}}(T^*) = \varrho\left[\left(\boldsymbol{\sigma_c}^{-1}\boldsymbol{\delta_c} + \boldsymbol{\sigma_n}^{-1}\boldsymbol{\delta_n}\right) B^*\right]. \tag{2.56}$$

The threshold interpretation follows from the standard next-generation-matrix criterion applied to the linearized spreading subsystem. □

Corollary 1. *Assume that all nodes have homogeneous parameters,*

$$\rho_i = \rho, \quad \delta_{c,i} = \delta_c, \quad \delta_{n,i} = \delta_n, \quad \sigma_{c,i} = \sigma_c, \quad \sigma_{n,i} = \sigma_n, \tag{2.57}$$

and that $T_i^* = \bar{T}$ for every node. Then,

$$\mathcal{R}_{\text{net}}(\bar{T}) = \rho\bar{T}\left(\frac{\delta_c}{\sigma_c} + \frac{\delta_n}{\sigma_n}\right)\varrho(A). \tag{2.58}$$

In particular, at the fully target network equilibrium, $\bar{T} = 1$,

$$\mathcal{R}_{0,\text{net}} = \rho\left(\frac{\delta_c}{\sigma_c} + \frac{\delta_n}{\sigma_n}\right)\varrho(A). \tag{2.59}$$

Proof. Under the stated assumptions, it is $B^* = \rho\bar{T}A^\top$ and

$$\boldsymbol{\sigma_c}^{-1}\boldsymbol{\delta_c} + \boldsymbol{\sigma_n}^{-1}\boldsymbol{\delta_n} = \left(\frac{\delta_c}{\sigma_c} + \frac{\delta_n}{\sigma_n}\right)I_N. \tag{2.60}$$

Because $\varrho(A^\top) = \varrho(A)$, the result follows directly from the previous proposition. □

2.5. The invasion threshold for the reduced system

For comparison with the full network formulation, we next consider a homogeneous, well-mixed, reduced model. This reduction is not intended to preserve the topology-dependent invasion threshold of the network system. Rather, it provides a low-dimensional representation in which the interaction term is approximated by the total spreading fraction. Consequently, the spectral factor $\varrho(A)$ appearing in the full network threshold is absent from the reduced model. The threshold derived below must therefore be interpreted as the invasion threshold of the homogeneous well-mixed reduction and not as the threshold of the original network system.

A diffusion-free equilibrium (DFE) is an equilibrium at which no individuals are actively spreading information about the advertised product. In the present model, this condition is characterized by

$$S_{c,i}^* = S_{n,i}^* = 0, \qquad i = 1, \ldots, N. \tag{2.61}$$

The target and inactive compartments may still contain individuals.

Theorem 1. *The steady states of the underlying system associated with the system (2.36)–(2.38) are the diffusion-free equilibrium points $E_{\bar{T}}^* = \left(\bar{T}, 0, 0, 1 - \bar{T}\right)$, where $0 \le \bar{T} \le 1$.*

Proof. Set

$$\begin{aligned} T'(t) &= -\rho T(t)\left(S_c(t) + S_n(t)\right), & (2.62)\\ S_c'(t) &= \delta_c\rho T(t)\left(S_c(t) + S_n(t)\right) - \sigma_c S_c(t), & (2.63)\\ S_n'(t) &= \delta_n\rho T(t)\left(S_c(t) + S_n(t)\right) - \sigma_n S_n(t)), & (2.64) \end{aligned}$$

the underlying system associated with (2.36)–(2.38). Then, the steady states are the solutions of the system of the following system of equations:

$$0 = -\rho T\left(S_c + S_n\right), \tag{2.65}$$

$$0 = \delta_c \rho T (S_c + S_n) - \sigma_c S_c, \tag{2.66}$$
$$0 = \delta_n \rho T (S_c + S_n) - \sigma_n S_n. \tag{2.67}$$

From (2.65), it follows that either $T = 0$ or $S_c + S_n = 0$. A direct computation shows that in both cases, it is verified that $S_c = S_n = 0$. As $I(t) = 1 - T(t) - S_c(t) - S_n(t)$ for every instant of time t, the steady states are of the form $E^*_{\bar{T}} = \left(\bar{T}, 0, 0, 1 - \bar{T}\right)$ with $0 \leq \bar{T} \leq 1$. □

Theorem 2 (Invasion threshold)**.** *Let $E^*_{\bar{T}} = (\bar{T}, 0, 0, 1 - \bar{T})$ with $0 \leq \bar{T} \leq 1$ be a diffusion-free equilibrium of the reduced system. The next-generation matrix associated with the spreading compartments S_c and S_n has spectral radius*

$$\mathcal{R}_{red}(\bar{T}) = \rho \bar{T} \left(\frac{\delta_c}{\sigma_c} + \frac{\delta_n}{\sigma_n} \right). \tag{2.68}$$

Hence, $\mathcal{R}_{red}(\bar{T}) < 1$ implies local decay of sufficiently small spreading perturbations transverse to the diffusion-free equilibrium manifold, whereas $\mathcal{R}_{red}(\bar{T}) > 1$ implies linear instability in a spreading direction.

In particular, at the fully target equilibrium $E^*_0 = (1, 0, 0, 0)$, the basic invasion reproduction number is

$$\mathcal{R}_{0,red} = \rho \left(\frac{\delta_c}{\sigma_c} + \frac{\delta_n}{\sigma_n} \right). \tag{2.69}$$

More generally, if the initial target fraction is $T_0 = T(0)$, the corresponding initial effective reproduction number is

$$\mathcal{R}_{\text{eff},red}(0) = \rho\, T_0 \left(\frac{\delta_c}{\sigma_c} + \frac{\delta_n}{\sigma_n} \right) = T_0\, \mathcal{R}_{0,red}. \tag{2.70}$$

Proof. Taking into account the next-generation method and considering the equations that describe the dynamics of spreaders, that is,

$$S_c'(t) = \delta_c \rho T(t) (S_c(t) + S_n(t)) - \sigma_c S_c(t), \tag{2.71}$$
$$S_n'(t) = \delta_n \rho T(t) (S_c(t) + S_n(t)) - \sigma_n S_n(t)), \tag{2.72}$$

we obtain

$$\mathcal{F}_c = \delta_c \rho T (S_c + S_n), \quad \mathcal{V}_c = \sigma_c S_c, \tag{2.73}$$
$$\mathcal{F}_n = \delta_n \rho T (S_c + S_n), \quad \mathcal{V}_n = \sigma_n S_n. \tag{2.74}$$

Thus,

$$\mathcal{F}_0 = \begin{pmatrix} \delta_c \rho T & \delta_c \rho T \\ \delta_n \rho T & \delta_n \rho T \end{pmatrix}, \quad \mathcal{V}_0 = \begin{pmatrix} \sigma_c & 0 \\ 0 & \sigma_n \end{pmatrix}, \tag{2.75}$$

and consequently, the next-generation matrix is given by

$$\left(\mathcal{F}_0 \cdot \mathcal{V}_0^{-1} \right)_{E^*_{\bar{T}}} = \begin{pmatrix} \frac{\delta_c \rho T^*_\infty}{\sigma_c} & \frac{\delta_c \rho T^*_\infty}{\sigma_n} \\ \frac{\delta_n \rho T^*_\infty}{\sigma_c} & \frac{\delta_n \rho T^*_\infty}{\sigma_n} \end{pmatrix}. \tag{2.76}$$

A simple computation shows that the spectral radius of this matrix is $\rho \bar{T} (\delta_c \sigma_n + \delta_n \sigma_c) / (\sigma_c \sigma_n)$, thus finishing. □

Note that the relationship between the invasion thresholds of the full network model and the homogeneous reduced system can be made explicit. Under the homogeneous assumptions considered above, at the fully target equilibrium, we have

$$\mathcal{R}_{0,\text{net}} = \rho\left(\frac{\delta_c}{\sigma_c} + \frac{\delta_n}{\sigma_n}\right)\varrho(A), \tag{2.77}$$

whereas the corresponding threshold for the reduced system is

$$\mathcal{R}_{0,\text{red}} = \rho\left(\frac{\delta_c}{\sigma_c} + \frac{\delta_n}{\sigma_n}\right). \tag{2.78}$$

Therefore,

$$\mathcal{R}_{0,\text{net}} = \mathcal{R}_{0,red}\,\varrho(A). \tag{2.79}$$

Thus, the reduced threshold captures the contribution of the local diffusion and deactivation parameters, whereas the additional factor $\varrho(A)$ accounts for the effect of network connectivity on the invasion process. This relation also emphasizes that $\mathcal{R}_{0,\text{red}}$ should not, in general, be interpreted as the invasion threshold of the full network model.

Theorem 3 (Final-size relation)**.** *Assume that $\sigma_c, \sigma_n > 0$, and let $(T(t), S_c(t), S_n(t))$ be a solution of the reduced system satisfying*

$$\lim_{t\to\infty} S_c(t) = \lim_{t\to\infty} S_n(t) = 0. \tag{2.80}$$

If $T_0 = T(0) > 0$, then the terminal target fraction

$$T_\infty = \lim_{t\to\infty} T(t) \tag{2.81}$$

satisfies the implicit final-size relation

$$\log\left(\frac{T_\infty}{T_0}\right) = -\rho\left[\frac{S_c(0)}{\sigma_c} + \frac{S_n(0)}{\sigma_n} + \left(\frac{\delta_c}{\sigma_c} + \frac{\delta_n}{\sigma_n}\right)(T_0 - T_\infty)\right]. \tag{2.82}$$

Therefore, the invasion threshold and the final campaign size describe different properties of the dynamics. In particular, $\mathcal{R}_0 > 1$ indicates the possibility of initial invasion near the fully target state, but it does not imply that $T_\infty = 0$.

Proof. Considering the first equation of the reduced system, and because $T_0 = T(0) > 0$ and $T(t) > 0$ for every finite t, division by $T(t)$ gives

$$\frac{T'(t)}{T(t)} = -\rho(S_c(t) + S_n(t)). \tag{2.83}$$

Integrating over $[0, \infty)$ and using $T(t) \to T_\infty$ as $t \to \infty$, we obtain

$$\log\left(\frac{T_\infty}{T_0}\right) = -\rho\left[\int_0^\infty S_c(t)\,dt + \int_0^\infty S_n(t)\,dt\right]. \tag{2.84}$$

On the other hand, using again the first equation of the system, the equations for the two spreading compartments can be written as follows:

$$S_c'(t) = -\delta_c T'(t) - \sigma_c S_c(t) \tag{2.85}$$
$$S_n'(t) = -\delta_n T'(t) - \sigma_n S_n(t). \tag{2.86}$$

Integrating the first of these identities over $[0, \infty)$ yields

$$S_c(\infty) - S_c(0) = -\delta_c(T_\infty - T_0) - \sigma_c \int_0^\infty S_c(t)\, dt. \tag{2.87}$$

By hypothesis, $S_c(t) \to 0$ as $t \to \infty$. Hence,

$$\sigma_c \int_0^\infty S_c(t)\, dt = S_c(0) + \delta_c(T_0 - T_\infty), \tag{2.88}$$

and therefore,

$$\int_0^\infty S_c(t)\, dt = \frac{S_c(0)}{\sigma_c} + \frac{\delta_c}{\sigma_c}(T_0 - T_\infty). \tag{2.89}$$

Proceeding analogously with the equation for $S_n(t)$ and using $S_n(t) \to 0$ as $t \to \infty$, we obtain

$$\int_0^\infty S_n(t)\, dt = \frac{S_n(0)}{\sigma_n} + \frac{\delta_n}{\sigma_n}(T_0 - T_\infty). \tag{2.90}$$

Finally, substituting Eqs (2.89) and (2.90) into Eq (2.84) gives

$$\log\left(\frac{T_\infty}{T_0}\right) = -\rho\left[\frac{S_c(0)}{\sigma_c} + \frac{S_n(0)}{\sigma_n} + \left(\frac{\delta_c}{\sigma_c} + \frac{\delta_n}{\sigma_n}\right)(T_0 - T_\infty)\right], \tag{2.91}$$

which is the desired final-size relation. □

The distinction between the invasion threshold and the subsequent evolution of the diffusion process is illustrated numerically in Figure 2. Two representative trajectories of the reduced system are shown, corresponding to an initially supercritical regime, $\mathcal{R}_{\text{eff},red}(0) > 1$, and an initially subcritical regime, $\mathcal{R}_{\text{eff},red}(0) < 1$, respectively. These simulations illustrate the transient behavior of the different compartments for the particular parameter values and initial conditions considered; they should not be interpreted as implying that $\mathcal{R}_{0,red} > 1$ necessarily leads to $T_\infty = 0$ nor that every spreading component must decrease monotonically whenever $\mathcal{R}_{\text{eff},red}(0) < 1$. Furthermore, take note that these simulations provide a numerical illustration of the result rather than an independent mathematical proof.

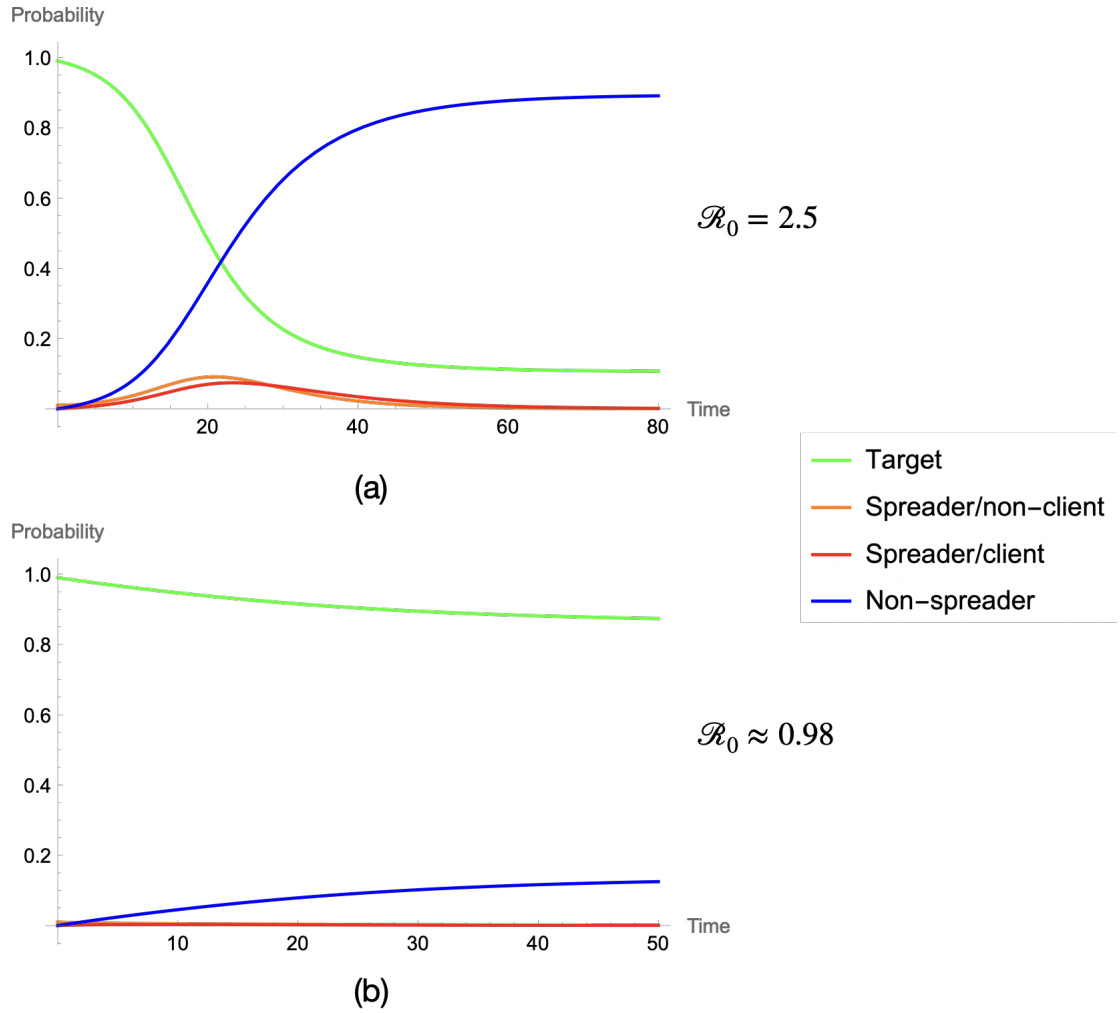


Figure 2. Evolution of the compartment probabilities in two representative simulations of the homogeneous reduced model: (a) Initially supercritical regime, $\mathcal{R}_{\text{eff},red}(0) > 1$; (b) Initially subcritical regime, $\mathcal{R}_{\text{eff,red}}(0) < 1$. The parameter values and initial conditions used in each simulation are indicated in the text.

To examine the relationship between the invasion threshold and the final campaign size in the homogeneous reduced model, we varied the transmission parameter ρ while keeping the branching probabilities, deactivation rates, and initial conditions fixed.

For each value of ρ, the reduced system was integrated numerically to approximate the terminal fractions T_∞ and I_∞. The corresponding basic invasion reproduction number was computed independently of the terminal state as

$$\mathcal{R}_{0,\text{red}} = \rho\left(\frac{\delta_c}{\sigma_c} + \frac{\delta_n}{\sigma_n}\right). \tag{2.92}$$

Figure 3 illustrates the dependence of the final target and inactive fractions on this parameter. The invasion threshold characterizes the initial growth or decay of sufficiently small spreading perturbations near a diffusion-free equilibrium; it does not imply that the final target fraction vanishes whenever

$\mathcal{R}_{0,\mathrm{red}} > 1$. Although increasing $\mathcal{R}_{0,\mathrm{red}}$ produces a progressively larger campaign reach in the parameter range considered, crossing the invasion threshold does not imply complete diffusion throughout the target population. In particular, for $\mathcal{R}_{0,\mathrm{red}} = 2.5$, the final-size relation gives $T_\infty \simeq 0.1059$. Thus, a positive fraction of the population may remain unreached even in the supercritical regime.

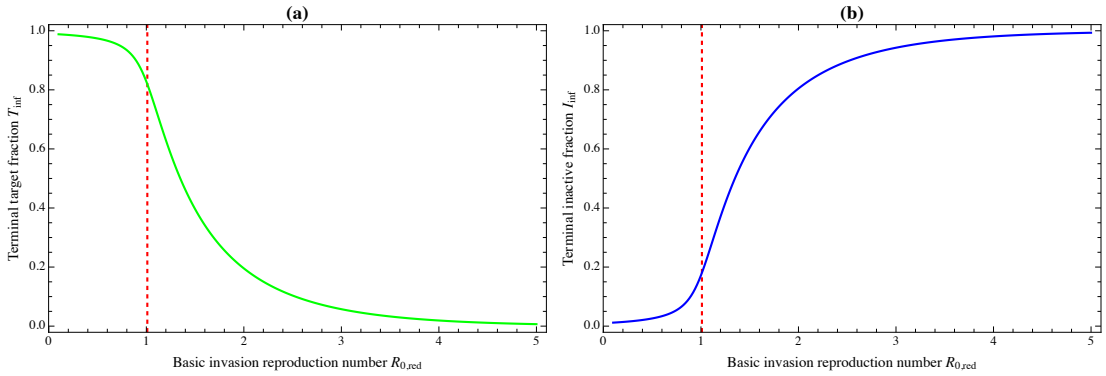


Figure 3. Final campaign size as a function of the basic invasion reproduction number $\mathcal{R}_{0,red}$ for the homogeneous reduced model: (a) Terminal target fraction T_∞; (b) Terminal inactive fraction $I_\infty = 1 - T_\infty$. The parameters are $\delta_c = 1$, $\delta_n = 0$, and $\sigma_c = 1$, with initial conditions $T(0) = 0.99$, $S_c(0) = 0.01$, and $S_n(0) = I(0) = 0$. The parameter ρ is varied so that $\mathcal{R}_{0,red} = \rho$. The vertical red dashed line indicates the initial invasion threshold $\mathcal{R}_{\mathrm{eff},red}(0) = 1$, corresponding to $\mathcal{R}_{0,red} = 1/T(0)$. The figure illustrates that the invasion threshold and the final campaign size are distinct concepts; $\mathcal{R}_{0,red} > 1$ does not imply $T_\infty = 0$.

In this simulation, the numerical computations were performed using `NDSolveValue` in `Wolfram Mathematica`, with the following specifications: `Method -> Automatic`, `AccuracyGoal -> 10`, `PrecisionGoal -> 10`, and `MaxSteps -> Infinity`. The integration interval was $[0, 500]$, with no prescribed fixed time step.

The parameters were fixed at $\delta_c = 1, \delta_n = 0, \sigma_c = \sigma_n = 1$, with initial conditions $T(0) = 0.99, S_c(0) = 0.01, S_n(0) = I(0) = 0$. The transmission parameter ρ was varied from 0.1 to 5 in increments of 0.02. For these parameter values, $\mathcal{R}_{0,\mathrm{red}} = \rho$. No random seed was required, as the numerical experiment involves the deterministic reduced system and does not use randomly generated networks or stochastic simulations.

2.6. Stochastic formulation and moment-closure approximation

In order to provide a precise stochastic interpretation of the deterministic individual-based model, we consider a continuous-time Markov chain describing the joint state of all individuals in the network.

Set $\mathcal{S} = \{T, S_c, S_n, I\}$, and define

$$X(t) = (X_1(t), \ldots, X_N(t)) \in \mathcal{S}^N, \tag{2.93}$$

where $X_i(t)$ denotes the state of the ith individual at time t. The joint process $X(t)$ is a continuous-time Markov chain on $\mathcal{S}^N$. Notice that in general, an individual coordinate $X_i(t)$ is not itself a Markov process, as its transition intensities depend on the states of its neighboring nodes.

For a network configuration $x = (x_1, \ldots, x_N) \in \mathcal{S}^N$, we define the diffusion pressure acting on ith node by

$$\lambda_i(x) = \rho_i \sum_{j=1}^{N} a_{ij} \mathbf{1}_{\{x_j \in \{S_c, S_n\}\}}. \tag{2.94}$$

The possible transitions of node i and their corresponding rates are the following:

$$T \longrightarrow S_c \quad \text{at rate } \delta_{c,i}\lambda_i(x), \tag{2.95}$$
$$T \longrightarrow S_n \quad \text{at rate } \delta_{n,i}\lambda_i(x), \tag{2.96}$$
$$T \longrightarrow I \quad \text{at rate } (1 - \delta_{c,i} - \delta_{n,i})\lambda_i(x), \tag{2.97}$$
$$S_c \longrightarrow I \quad \text{at rate } \sigma_{c,i}, \tag{2.98}$$
$$S_n \longrightarrow I \quad \text{at rate } \sigma_{n,i}. \tag{2.99}$$

Note that no other transitions are allowed.

For a function $f : \mathcal{S}^N \to \mathbb{R}$, the infinitesimal generator $\mathcal{L}$ of the joint Markov chain is given by

$$\begin{aligned}(\mathcal{L}f)(x) = &\sum_{i:x_i=T} \delta_{c,i}\lambda_i(x)\left[f(x^{i\to S_c}) - f(x)\right] + \sum_{i:x_i=T} \delta_{n,i}\lambda_i(x)\left[f(x^{i\to S_n}) - f(x)\right] \\ &+ \sum_{i:x_i=T} (1 - \delta_{c,i} - \delta_{n,i})\lambda_i(x)\left[f(x^{i\to I}) - f(x)\right] \\ &+ \sum_{i:x_i=S_c} \sigma_{c,i}\left[f(x^{i\to I}) - f(x)\right] + \sum_{i:x_i=S_n} \sigma_{n,i}\left[f(x^{i\to I}) - f(x)\right],\end{aligned} \tag{2.100}$$

where $x^{i\to\alpha}$ denotes the configuration obtained from x by changing only the state of the ith node to α.

For each node i and state $\alpha \in \mathcal{S}$, define the indicator variable $X_i^\alpha(t) = \mathbf{1}_{\{X_i(t)=\alpha\}}$ such that

$$\sum_{\alpha\in\mathcal{S}} X_i^\alpha(t) = 1 \quad \text{(almost surely)}. \tag{2.101}$$

The corresponding marginal probabilities are

$$T_i(t) = \mathbb{E}[X_i^T(t)], \quad S_{c,i}(t) = \mathbb{E}[X_i^{S_c}(t)], \tag{2.102}$$
$$S_{n,i}(t) = \mathbb{E}[X_i^{S_n}(t)], \quad I_i(t) = \mathbb{E}[X_i^I(t)]. \tag{2.103}$$

Applying the Kolmogorov forward equations or equivalently, the generator identity

$$\frac{d}{dt}\mathbb{E}[f(X(t))] = \mathbb{E}[(\mathcal{L}f)(X(t))] \tag{2.104}$$

to the indicator variables gives the following exact marginal equations:

$$\frac{dT_i}{dt} = -\rho_i \sum_{j=1}^{N} a_{ji}\mathbb{E}\left[X_i^T\left(X_j^{S_c} + X_j^{S_n}\right)\right], \tag{2.105}$$

$$\frac{dS_{c,i}}{dt} = \delta_{c,i}\rho_i \sum_{j=1}^{N} a_{ji}\mathbb{E}\left[X_i^T\left(X_j^{S_c} + X_j^{S_n}\right)\right] - \sigma_{c,i}S_{c,i}, \tag{2.106}$$

$$\frac{dS_{n,i}}{dt} = \delta_{n,i}\rho_i \sum_{j=1}^{N} a_{ji}\mathbb{E}\left[X_i^T\left(X_j^{S_c} + X_j^{S_n}\right)\right] - \sigma_{n,i}S_{n,i}, \tag{2.107}$$

$$\frac{dI_i}{dt} = (1-\delta_{c,i}-\delta_{n,i})\rho_i \sum_{j=1}^{N} a_{ji}\mathbb{E}\left[X_i^T\left(X_j^{S_c} + X_j^{S_n}\right)\right] + \sigma_{c,i}S_{c,i} + \sigma_{n,i}S_{n,i}. \tag{2.108}$$

These equations are not closed at the level of single-node marginal probabilities, as they involve pairwise moments associated with neighboring nodes. To obtain a closed deterministic system, we adopt the first-order mean-field approximation

$$\mathbb{E}\left[X_i^T X_j^{S_c}\right] \approx \mathbb{E}[X_i^T]\,\mathbb{E}[X_j^{S_c}] = T_i S_{c,j} \tag{2.109}$$

and

$$\mathbb{E}\left[X_i^T X_j^{S_n}\right] \approx \mathbb{E}[X_i^T]\,\mathbb{E}[X_j^{S_n}] = T_i S_{n,j}. \tag{2.110}$$

As a consequence,

$$\mathbb{E}\left[X_i^T\left(X_j^{S_c} + X_j^{S_n}\right)\right] \approx T_i\left(S_{c,j} + S_{n,j}\right). \tag{2.111}$$

Substitution of this approximation into the exact marginal equations yields precisely the deterministic system (2.16)–(2.19).

3. Numerical simulations

3.1. Computational setup and reproducibility

The numerical experiments were performed by integrating the individual-based mean-field system on synthetic social networks. Unless otherwise specified, the network topology was represented by a simple, connected, undirected graph, consistent with the graph-theoretic formulation introduced in Section 2.1.

Barabási–Albert networks were generated using a preferential-attachment algorithm. The parameter m denotes the number of edges added with each new node, whereas N denotes the total number of nodes. All network-dependent quantities were computed directly from the generated adjacency matrices.

The differential equations were solved numerically using `NDSolve` of `Wolfram Mathematica`. For simulations initiated by a single spreading client, the initial conditions were

$$T_i(0) = \begin{cases} 0, & i = i_0, \\ 1, & i \neq i_0, \end{cases} \qquad S_{c,i}(0) = \begin{cases} 1, & i = i_0, \\ 0, & i \neq i_0, \end{cases} \tag{3.1}$$

and $S_{n,i}(0) = I_i(0) = 0$, with $i = 1, \ldots, N$, where i_0 denotes the initially spreading node. Unless otherwise indicated, this node was selected as a node of maximum degree.

For experiments involving multiple graph realizations, independent networks were generated for each parameter configuration, and the reported results include the corresponding sample means and measures of variability.

To ensure that individual parameter effects can be identified, comparative experiments were designed by holding the network realization, initial conditions, and all other model parameters fixed while varying the parameter or parameter group under investigation.

The `Mathematica` files can be downloaded from https://zenodo.org/records/23433360.

3.2. Illustrative numerical examples

In what follows, some simulations are presented. Because the proposed model is formulated as a system of ordinary differential equations, time is continuous, and no intrinsic discrete time step is associated with the model. In the numerical simulations, the system was solved using an adaptive-step numerical ODE solver (`NDSolve` of Mathematica); hence, the integration time step was automatically selected and adjusted by the solver according to its error-control criteria. The integer values of t displayed in some figures and tables (e.g., $t = 0, 1, 2, \ldots$) correspond only to sampling times at which the numerical solution is reported and should not be interpreted as the integration time step. Unless otherwise specified, time is expressed in arbitrary time units, as the model parameters have not been calibrated to a particular empirical campaign. Accordingly, ρ_i, $\sigma_{c,i}$, and $\sigma_{n,i}$ are rates expressed in inverse time units, whereas $\delta_{c,i}$ and $\delta_{n,i}$ are dimensionless transition fractions.

Specifically, the following are computed:

1. The temporal and global evolution of the probabilities of different individuals.
2. The temporal and local evolution of the probabilities of all nodes/individuals of the network.
3. The temporal and global evolution of the sum of the different probabilities of all nodes.
4. The evolution of the number of nodes/individuals with different highest probabilities.
5. The temporal evolution of the number of nodes/individuals with the highest probabilities of being target and spreader, considering different initial spreader nodes.

These can be considered as the simulations that best illustrate the behavior of the system.

Assume that the contact topology is defined by a scale-free network composed of $N = 100$ nodes, where $m = 1$ denotes the number of edges by which each newly added node is connected to existing nodes in the Barabási–Albert preferential-attachment algorithm. For the sake of simplicity, suppose that all individuals are endowed with the same epidemiological coefficients, namely

$$\rho_i = 0.75, \quad \delta_{c,i} = 0.4, \quad \delta_{n,i} = 0.2, \quad \sigma_{c,i} = 0.1, \quad \sigma_{n,i} = 0.1. \tag{3.2}$$

Unless otherwise stated, the network simulations are initialized with a single spreading client at node i_0 (which corresponds to the highest degree centrality), and all remaining individuals are initially targets. More precisely,

$$(T_{i_0}(0), S_{c,i_0}(0), S_{n,i_0}(0), I_{i_0}(0)) = (0, 1, 0, 0), \tag{3.3}$$

and

$$(T_i(0), S_{c,i}(0), S_{n,i}(0), I_i(0)) = (1, 0, 0, 0), \qquad i \neq i_0. \tag{3.4}$$

In Figure 4, we can observe the evolution of the different probabilities for each individual of the population. Figure 4-(a) depicts all probabilities (for different devices) of being the target of the advertising campaign at time t. The probabilities of being a spreading client or nonclient are shown in Figure 4-(b) and 4-(c), respectively. Finally, Figure 4-(d) displays the probabilities of being aware of the product and not advertising it.

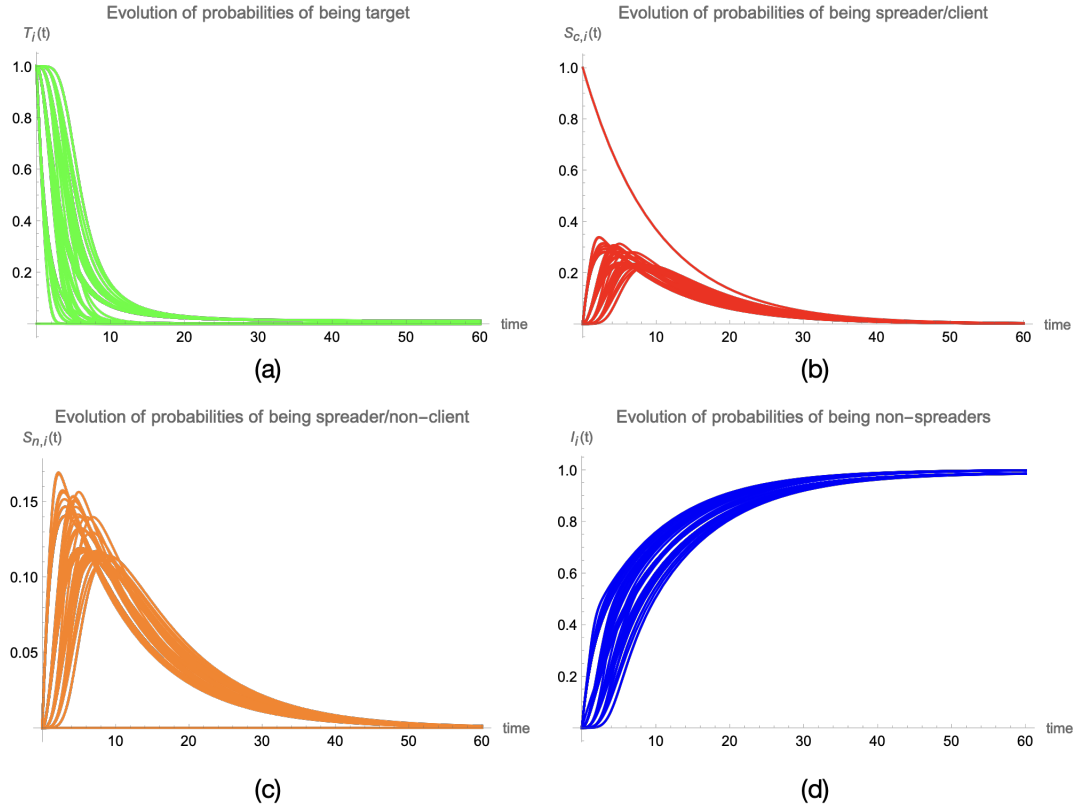


Figure 4. Temporal evolution of the different probabilities in a scale-free complex network with $m = 1$ and $\rho_i = 0.75, \delta_{c,i} = 0.4, \delta_{n,i} = 0.2, \sigma_{c,i} = 0.1, \sigma_{n,i} = 0.1$: (a) Evolution of the probabilities to be target. (b) Temporal evolution of the probabilities to be spreader/client. (c) Temporal evolution of the probabilities to be spreader/nonclient. (d) Temporal evolution of the probabilities to be nonspreader (client or nonclient).

3.3. Expected compartment sizes and most-probable-state classification

Because each node i is represented by the probability vector

$$\mathbf{p}_i(t) = (T_i(t), S_{c,i}(t), S_{n,i}(t), I_i(t)), \tag{3.5}$$

two different population-level quantities can be considered.

First, the expected compartment sizes predicted by the individual-based mean-field approximation are given by

$$\overline{N}_T(t) = \sum_{i=1}^{N} T_i(t),\ \overline{N}_{S_c}(t) = \sum_{i=1}^{N} S_{c,i}(t),\ \overline{N}_{S_n}(t) = \sum_{i=1}^{N} S_{n,i}(t),\ \overline{N}_I(t) = \sum_{i=1}^{N} I_i(t). \tag{3.6}$$

In particular, the expected total number of spreading individuals is approximated by

$$\overline{N}_S(t) = \sum_{i=1}^{N} \left(S_{c,i}(t) + S_{n,i}(t)\right). \tag{3.7}$$

These quantities correspond to the sums of the node-level marginal probabilities. They provide mean-field approximations to the expected compartment sizes of the underlying stochastic process and satisfy

$$\overline{N}_T(t) + \overline{N}_{S_c}(t) + \overline{N}_{S_n}(t) + \overline{N}_I(t) = N. \tag{3.8}$$

Second, a node can be assigned a most probable state by applying the classification rule

$$\widehat{X}_i(t) = \underset{\alpha\in\{T,S_c,S_n,I\}}{\arg\max}\ p_{i,\alpha}(t), \tag{3.9}$$

with ties resolved according to a fixed predetermined ordering of the states. Consquently, the number of nodes classified in state α is

$$C_\alpha(t) = \sum_{i=1}^{N} \mathbf{1}_{\{\widehat{X}_i(t)=\alpha\}}. \tag{3.10}$$

Unlike the expected compartment sizes, $C_\alpha(t)$ is a classification count. It depends only on which probability is largest and not on its magnitude. Consequently, this quantity may change discontinuously when the most probable state of a node changes, even though the underlying probability trajectories are continuous.

The numerical experiments below distinguish between these two quantities. Expected compartment sizes are used to quantify the population-level diffusion dynamics, whereas most-probable-state classifications are retained when the objective is to visualize or compare the dominant predicted states of individual nodes.

Figure 5 illustrates the most-probable-state classification of the nodes at three selected times, $t = 0$, $t = 2$, and $t = 4$. The first column displays the classification obtained by comparing the four individual probabilities $T_i(t)$, $S_{c,i}(t)$, $S_{n,i}(t)$, and $I_i(t)$. That is, each node is classified according to the largest component of its four-state probability vector $(T_i, S_{c,i}, S_{n,i}, I_i)$. The second column considers three aggregated categories: target, spreader, and inactive. In this case, the spreading probability is defined as $S_i(t) = S_{c,i}(t) + S_{n,i}(t)$, and each node is assigned to the category corresponding to the largest value among $T_i(t)$, $S_i(t)$, and $I_i(t)$. These two classification procedures need not assign the same category to a given node.

The colors therefore indicate the most probable state or aggregated category of each node rather than its actual stochastic state. In particular, the resulting classification should not be interpreted as a direct measurement of the expected number of individuals in each compartment.

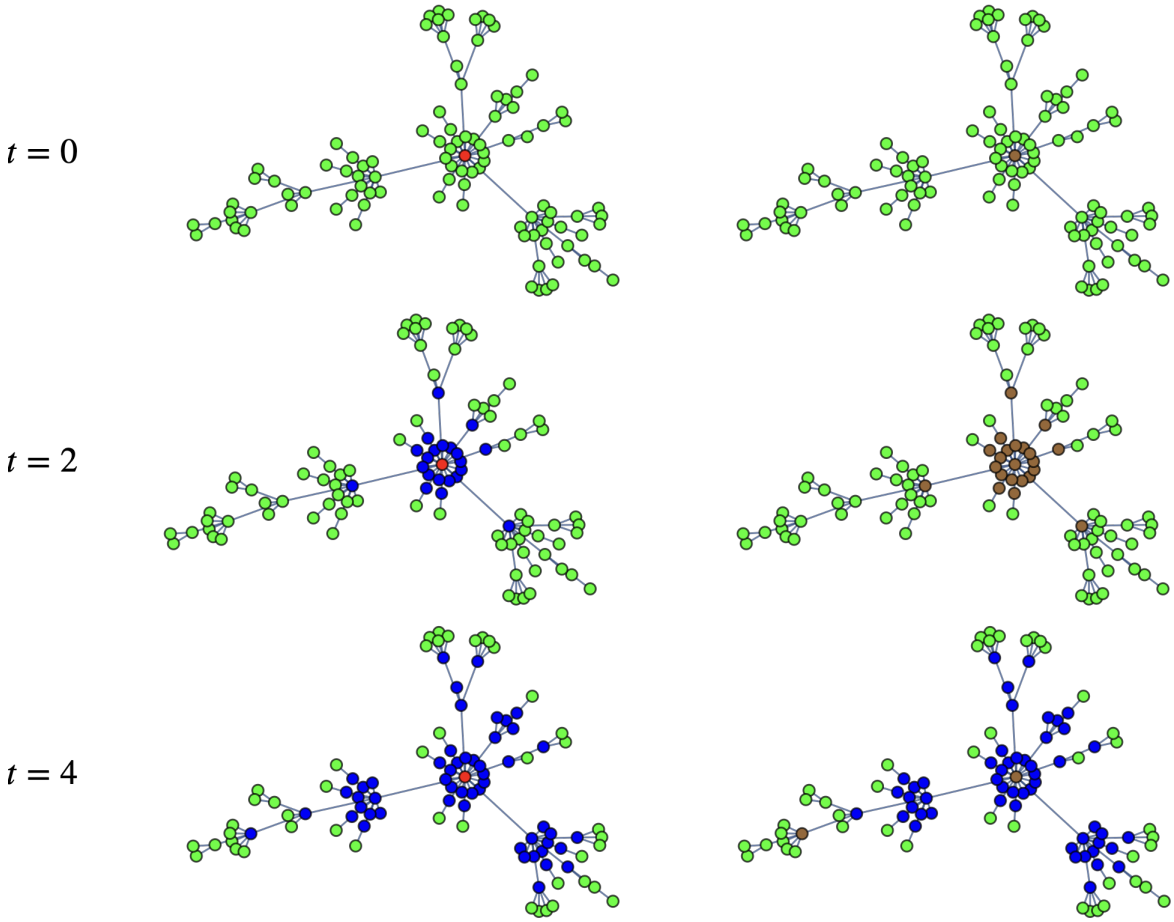


Figure 5. Most-probable-state classification of the network nodes at times $t = 0, 2, 4$. Left column: Classification based on the four probabilities T_i, $S_{c,i}$, $S_{n,i}$, and I_i. Right column: Classification based on the three aggregated probabilities T_i, $S_{c,i} + S_{n,i}$, and I_i. The colors indicate the categories defined by each classification rule, not the actual stochastic states of the nodes.

Figure 6 shows the temporal evolution of the number of nodes classified according to their most probable state. Initially, almost all individuals are classified as targets, whereas only the initially activated node is classified as a spreading client. As the advertising information propagates through the network, the number of nodes classified as targets decreases, while the number classified as inactive (nonspreading) individuals increases. Eventually, all nodes are classified as inactive, illustrating the progressive cessation of spreading activity in this numerical experiment. It is worth emphasizing that these curves represent counts obtained by assigning each node to the state with the highest probability at each time, rather than expected compartment sizes. In particular, the absence of nodes classified as spreading clients or spreading nonclients does not necessarily imply that their corresponding probabilities are zero.

To isolate the influence of the branching probabilities, we consider two parameter configurations on the same realization of a Barabási–Albert network, with $N = 100$, $m = 2$, and

$$\rho_i = 0.75, \quad \sigma_c = 0.1, \quad \sigma_n = 0.1. \tag{3.11}$$

Note that the transmission and deactivation rates, the adjacency matrix, and the initial conditions are identical in both experiments. In the first configuration, $(\delta_c, \delta_n) = (0.4, 0.2)$, whereas in the second configuration, $(\delta_c, \delta_n) = (0.5, 0.4)$. Finally, the initial spreading node is one of maximum degree, and its initial state is S_c, whereas all other nodes begin in state T.

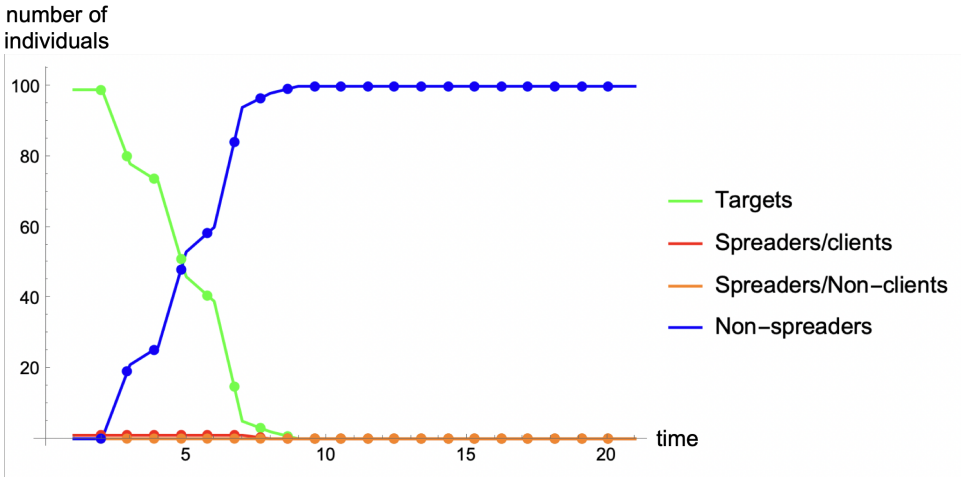


Figure 6. Temporal evolution of the number of nodes classified according to their most probable state. The curves represent classification counts rather than expected compartment sizes.

The resulting trajectories are compared using the expected number of spreading individuals,

$$\mathbb{E}[N_S(t)] = \sum_{i=1}^{N} \left(S_{c,i}(t) + S_{n,i}(t)\right). \tag{3.12}$$

Because all other experimental conditions are unchanged, any observed differences between the two deterministic trajectories can be attributed to the joint modification of the branching probabilities. The comparison does not, however, distinguish the individual contributions of δ_c and δ_n.

Because $\sigma_c = \sigma_n$ in both scenarios, the evolution of the total spreading probability $S_i(t) = S_{c,i}(t) + S_{n,i}(t)$ depends on the branching probabilities only through their sum $\delta_c + \delta_n$. Consequently, the comparison specifically examines the effect of increasing the total probability of becoming a spreader from 0.6 to 0.9.

The results of this comparison are shown in Figure 7. Both scenarios exhibit an initial increase in the expected number of spreading individuals, followed by a progressive decline after reaching their respective maxima. However, the magnitude and timing of the peaks differ substantially.

In Scenario A, with $(\delta_c, \delta_n) = (0.4, 0.2)$, the expected number of spreading individuals reaches a maximum of approximately 45 at $t \approx 3.7$. In contrast, Scenario B, with $(\delta_c, \delta_n) = (0.5, 0.4)$, reaches a maximum of approximately 72 at $t \approx 2.8$. Thus, the simultaneous increase in the branching probabilities produces a higher and earlier peak of spreading activity in the network considered.

The difference between the two scenarios remains visible at the end of the simulation interval. At $t = 20$, the expected numbers of spreading individuals are approximately 10.02 and 14.03 for Scenarios A and B, respectively. These values correspond to the number of active spreaders at the final observation time rather than to the cumulative number of individuals reached by the campaign.

Because both trajectories were obtained using the same realization of the network, the same initial conditions, and identical transmission and deactivation rates, the observed differences can be attributed to the joint modification of δ_c and δ_n rather than to changes in network topology. Nevertheless, this experiment does not distinguish the individual contributions of the two branching probabilities.

Overall, the numerical results illustrate that for the fixed network and parameter configurations considered here, increasing the probabilities of becoming a spreading client or a spreading nonclient leads to a more pronounced and earlier peak in spreading activity, together with a larger number of active spreaders throughout the later stages of the simulated interval.

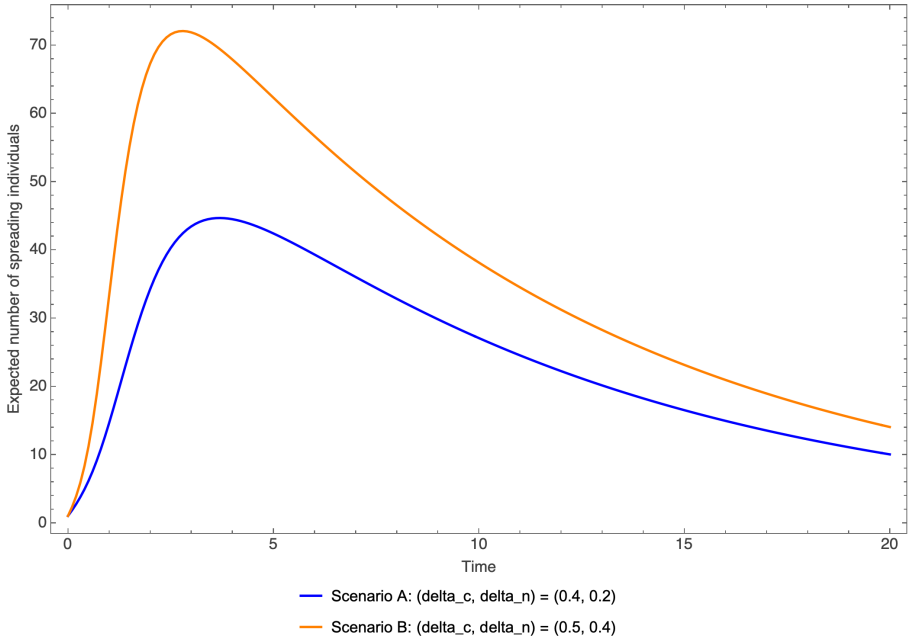


Figure 7. Evolution of the expected number of spreading individuals in two scenarios with different branching probabilities on the same realization of a Barabási–Albert network ($N = 100$, $m = 2$). Scenario A (blue): $(\delta_c, \delta_n) = (0.4, 0.2)$. Scenario B (orange): $(\delta_c, \delta_n) = (0.5, 0.4)$.

Now, we test how varying the defining characteristic of the initial spreader affects the dynamics. We will consider different centrality measures: the previously used degree centrality, closeness centrality, betweenness centrality, eigenvector centrality, eccentricity, and clustering coefficient. Suppose the population of $n = 500$ individuals is interconnected according to a scale-free network with $k = 3$, and the considered epidemiological coefficients are as follows:

$$\rho_i = 0.6, \quad \delta_{c,i} = 0.6, \quad \delta_{n,i} = 0.3, \quad \sigma_{c,i} = 0.1, \quad \sigma_{n,i} = 0.25. \tag{3.13}$$

In Figure 8, this network is depicted, where the nodes with the highest structural indices are highlighted in red (eccentricity), blue (eigenvector centrality, which coincides with degree centrality, closeness, and betweenness), and purple (clustering coefficient). Specifically, the main structural values of these nodes are shown in Table 1. Additionally, the main structural characteristics of the network are introduced in Table 2.

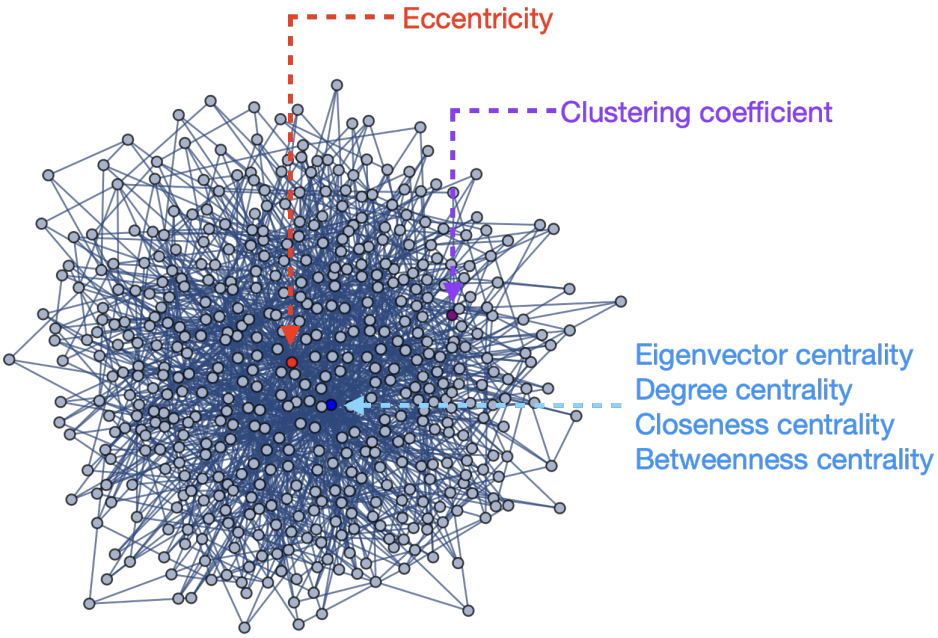


Figure 8. Scale-free network defined by $m = 3$ and $N = 500$ nodes, where the initial spreader nodes are highlighted in different colors.

Table 1. Main structural indices of the nodes which are spreaders at $t = 0$.

Node (highest structural indices)	Degree centrality	**Eccentricity**	Closeness	Betweenness	Clustering
4 (degree, closeness, betweenness)	**0.1583**	0.2500	**0.4664**	**0.1943**	0.0162
10 (eccentricity)	0.1443	**0.3333**	0.4599	0.1790	0.0121
214 (clustering)	0.0060	0.2500	0.3404	0.0004	**0.6667**

Table 2. Main global structural indices of the scale-free network.

Density	Diameter	Radius	Global clustering	Mean clustering	Mean degree
0.0120	5	3	0.0259	0.0454	6

In Figures 9 and 10, the temporal evolutions of the number of individuals whose highest probability is of being a target or spreaders (client or nonclient) at time t are shown, respectively. Explicit numerical values of these evolutions are provided in Tables 3 and 4.

It can be observed from these simulations that the behavior over time of the number of individuals with the highest probability of being spreaders is exactly the same when the only initially spreading individual is characterized by having the highest degree centrality, closeness centrality, betweenness coefficient, and eigenvector centrality. This is because in this type of network, these characteristics focus on the same node (defined by $i = 4$). On the other hand, slight differences appear when the propagation process starts with the individual characterized by the highest eccentricity, and finally, these differences are accentuated when the initially spreading individual has the highest clustering

coefficient. In this latter case, it can be observed how the spreading process slows down, although the maximum is still reached.

Table 3. Temporal evolution of the number of individuals with the highest probability of being target.

Initial spreader characteristic	$t = 0$	$t = 1$	$t = 2$	$t = 3$	$t = 4$	$t = 5$
Degree	499	404	0	0	0	0
Closeness	499	404	0	0	0	0
Betweenness	499	404	0	0	0	0
Eccentricity	499	404	0	0	0	0
Eigenvector	499	404	0	0	0	0
Clustering	499	479	12	0	0	0

Table 4. Temporal evolution of the number of individual whose highest probability is of being spreader (client or nonclient).

Initial spreader characteristic	$t = 0$	$t = 1$	$t = 2$	$t = 3$	$t = 4$	$t = 5$	$t = 6$	$t = 7$
Degree	1	96	500	500	455	4	1	0
Closeness	1	96	500	500	455	4	1	0
Betweenness	1	96	500	500	455	4	1	0
Eccentricity	1	96	500	500	462	3	1	0
Eigenvector	1	96	500	500	455	4	1	0
Clustering	1	21	488	500	494	81	1	0

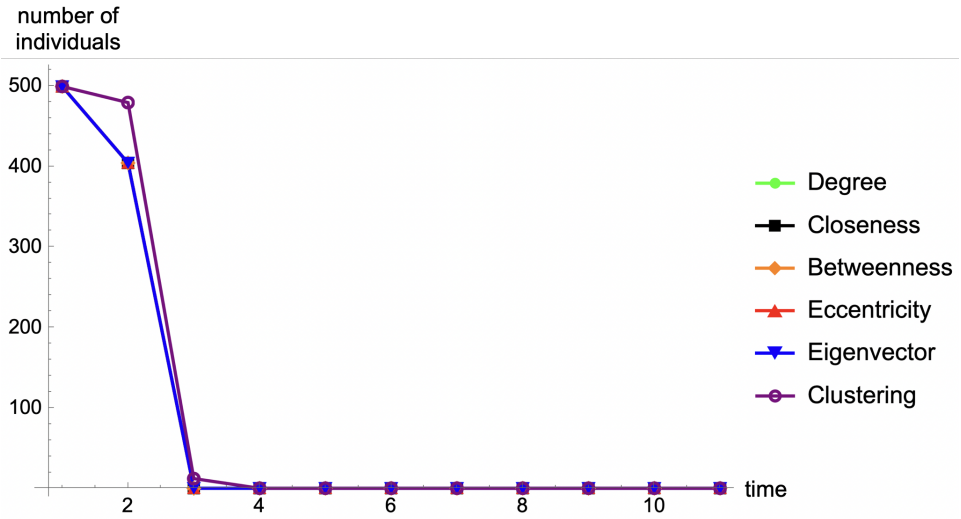


Figure 9. Temporal evolution of the number of nodes classified as targets according to the most-probable-state rule for different choices of the initially spreading node.

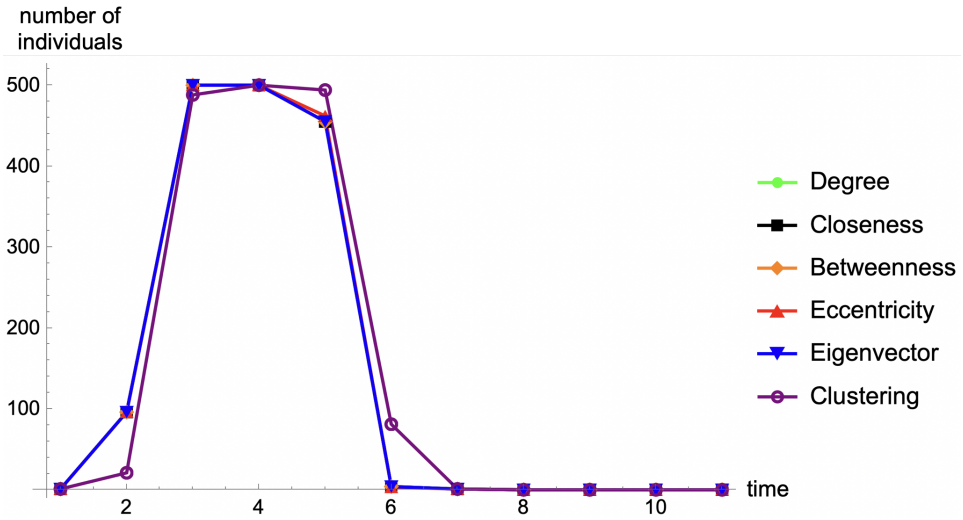


Figure 10. Temporal evolution of the number of nodes classified as spreaders according to the aggregated most-probable-state rule for different choices of the initially spreading node.

Finally, we test what happens with the viral marketing spread when the coefficient m of the BA algorithm generating the scale-free network is varied. Different networks have been generated for different values of m (shown in Figure 11), and the temporal evolution of the number of nodes with the highest probability of being spreaders at each instant of time has been computed. Table 5 shows the main structural indices of these networks. In this way, Figure 12 demonstrates how the evolutions in cases considering $m \geq 2$ are very similar, although with a higher value of k, we reach a maximum number of spreaders for a more extended period, and the descent to equilibrium occurs sooner. This trend in the descent towards equilibrium is more pronounced with larger values of m. A noteworthy case is when $m = 1$, where the spreading process (as observed in the green line in Figure 12) is much less aggressive and progresses at a slower pace.

Table 5. Main global structural indices of the scale-free networks employed in the simulations.

m	Density	Diameter	Radius	Global clustering	Mean clustering	Mean degree
$m = 1$	0.02	9	5	0	0	1.98
$m = 2$	0.0398	6	3	0.0721	0.1098	3.9402
$m = 3$	0.0594	4	3	0.1010	0.2310	5.8806
$m = 4$	0.0788	4	3	0.1372	0.1805	7.8012
$m = 5$	0.0980	4	2	0.1737	0.1949	9.702

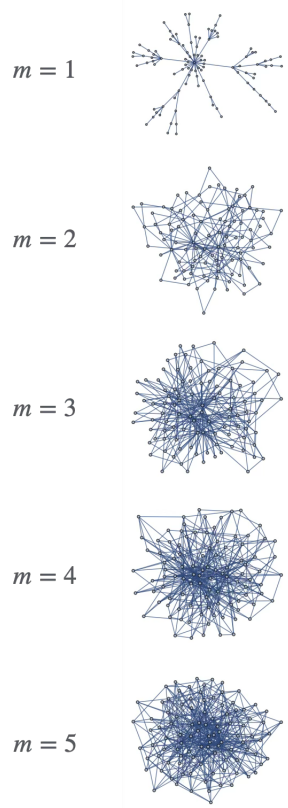


Figure 11. Scale-free networks used in the simulations.

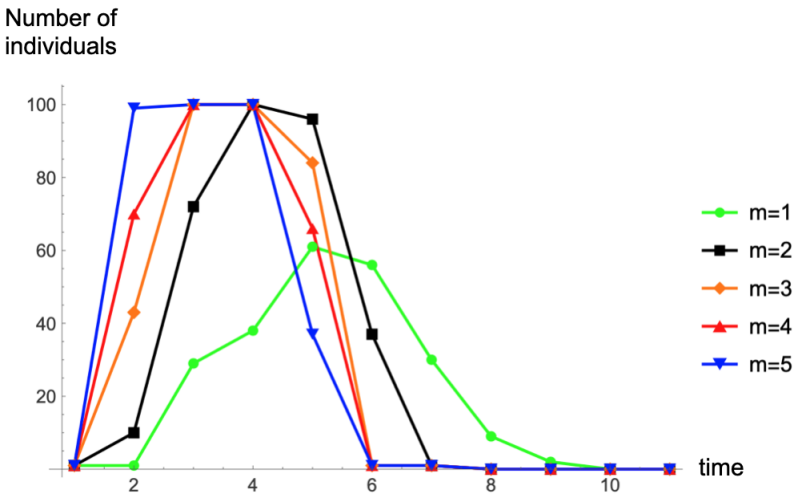


Figure 12. Temporal evolution of the number of nodes classified as spreaders according to the most-probable-state rule for Barabási–Albert networks with different attachment parameters $m = 1, 2, 3, 4, 5$. A node is classified as a spreader when its aggregated spreading probability $S_{c,i}(t) + S_{n,i}(t)$ is greater than both $T_i(t)$ and $I_i(t)$. The curves represent classification counts rather than expected compartment sizes.

3.4. Validation of the mean-field approximation

To quantify the accuracy of the first-order moment closure, we compare the deterministic marginal probabilities with Monte Carlo estimates obtained from independent realizations of the continuous-time Markov chain. For each state $\alpha \in \mathcal{S}$, we compute

$$E_\alpha = \frac{1}{N(K+1)} \sum_{i=1}^{N} \sum_{k=0}^{K} \left| p_{i,\alpha}(t_k) - \widehat{p}_{i,\alpha}(t_k) \right|, \tag{3.14}$$

where $p_{i,\alpha}(t_k)$ denotes the deterministic marginal probability, and $\widehat{p}_{i,\alpha}(t_k)$ is its Monte Carlo estimate.

Two complementary numerical experiments were performed. In all cases, the parameters of the diffusion process were fixed at

$$\rho = 0.75, \quad \delta_c = 0.4, \quad \delta_n = 0.2, \quad \sigma_c = \sigma_n = 0.1, \tag{3.15}$$

and the stochastic estimates were obtained from $M = 1000$ independent realizations of the continuous-time Markov chain. The deterministic and stochastic models were initialized consistently, with a single initial spreader and all remaining nodes in the target state. The initial spreader was chosen as a node of maximum degree. The time interval $[0, 10]$ was considered, and the marginal probabilities were compared at sampling times separated by $\Delta t = 0.1$.

First, we investigated how the accuracy of the first-order closure changes with network connectivity. Barabási–Albert networks with $N = 50$ nodes and attachment parameters $m = 1, 2, 3$ were considered. The corresponding mean degrees were 1.96, 3.88, and 5.76, respectively. Table 6 reports the network characteristics and the mean absolute errors obtained for the four states.

Table 6. Comparison between the deterministic mean-field approximation and Monte Carlo estimates for Barabási–Albert networks with different levels of connectivity. Each Monte Carlo estimate was obtained from 1000 independent realizations of the continuous-time Markov chain.

m	$\langle d \rangle$	Density	Clustering	E_T	E_{S_c}	E_{S_n}	E_I
1	1.96	0.0400	0	0.302835	0.089053	0.045155	0.169544
2	3.88	0.07918	0.18695	0.121868	0.033486	0.017284	0.075113
3	5.76	0.11755	0.21614	0.074571	0.023167	0.011412	0.047454

A clear decrease in the approximation error is observed as k increases. In fact, the errors decrease monotonically for all four states in the three networks considered. For example, the error associated with the target state decreases from $E_T = 0.302835$ for $m = 1$ to $E_T = 0.074571$ for $m = 3$. Thus, for this family of Barabási–Albert networks, the first-order mean-field approximation becomes substantially more accurate as network connectivity increases.

It should be emphasized, however, that changing the attachment parameter k simultaneously modifies several structural properties of the network, including its mean degree, density, and clustering. Consequently, the preceding experiment cannot be used to attribute the observed improvement to any single network property. To examine more specifically the effect of local clustering, a second numerical experiment was therefore performed.

For this purpose, Watts–Strogatz-type networks with $N = 50$ and $N = 100$ nodes were constructed with mean degree $\langle d \rangle = 4$. For each network size, two rewiring regimes were considered: $p = 0.05$, which preserves a strongly clustered local structure, and $p = 1$, which produces a substantially less clustered network. Importantly, for a fixed value of N, the number of edges, mean degree, and density were kept unchanged so that the comparison primarily reflects differences in network organization and local clustering. The resulting errors are reported in Table 7.

Table 7. Comparison between the deterministic mean-field approximation and Monte Carlo estimates for networks with different clustering levels. The mean degree is fixed at $\langle d \rangle = 4$, and each Monte Carlo estimate is based on 1000 independent realizations.

N	p	Density	Clustering	E_T	E_{S_c}	E_{S_n}	E_I
50	0.05	0.08163	0.41667	0.400208	0.115462	0.058298	0.227060
50	1.00	0.08163	0.09752	0.198395	0.053491	0.026655	0.120233
100	0.05	0.04040	0.43767	0.429337	0.128935	0.065001	0.235702
100	1.00	0.04040	0.02009	0.240003	0.062994	0.032258	0.146601

For both network sizes, the approximation errors are substantially larger in the highly clustered networks. For $N = 50$, for example, the target-state error decreases from $E_T = 0.400208$ for $p = 0.05$ to $E_T = 0.198395$ for $p = 1$. A similar behavior is observed for $N = 100$, where the corresponding values are 0.429337 and 0.240003. The same qualitative behavior is observed for the other three states.

The terminal target fractions also illustrate the direction of the discrepancy. For $N = 50$ and $p = 0.05$, the deterministic approximation gives $T(10) = 0.000408$, whereas the Monte Carlo estimate is 0.5905. For $p = 1$, these values are 0.001134 and 0.17304, respectively. Similarly, for $N = 100$, the deterministic and Monte Carlo values are 0.001431 and 0.77256 for $p = 0.05$ and 0.001261 and 0.20353 for $p = 1$. Thus, in the network regimes considered here, the first-order deterministic closure tends to overestimate the overall extent of the diffusion process, particularly in highly clustered networks.

These observations are consistent with the nature of the first-order moment-closure approximation. The factorization

$$\mathbb{E}\left[X_i^T X_j^\alpha\right] \approx \mathbb{E}\left[X_i^T\right]\mathbb{E}\left[X_j^\alpha\right], \quad \alpha \in \{S_c, S_n\}, \tag{3.16}$$

neglects dynamical correlations between neighboring nodes. Such correlations may become particularly relevant in sparse or strongly clustered networks, where the local state of a node is more strongly related to the states of its neighbors. The numerical results are therefore consistent with the loss of pairwise correlations inherent in the first-order closure.

It is also worth noting that increasing the number of nodes from $N = 50$ to $N = 100$ does not by itself improve the approximation in the experiments considered here. Because the mean degree is kept fixed at $\langle d \rangle = 4$, increasing N does not increase the local connectivity of individual nodes. Thus, network size alone should not be expected to eliminate the correlations neglected by the first-order closure.

Overall, these experiments show that the deterministic system provides a topology-dependent approximation to the exact stochastic marginal dynamics. Its accuracy improves substantially for the more connected Barabási–Albert networks considered here, whereas larger discrepancies are observed in sparse or highly clustered network structures. The first-order mean-field model should therefore be

interpreted as an approximation whose accuracy depends on the structural properties of the underlying network rather than as an exact representation of the marginal probabilities of the stochastic process.

4. Conclusions and future work

Mathematical models of viral marketing diffusion have frequently been formulated using population-level compartmental approaches. Although these models provide valuable information about the overall propagation process, network-based formulations offer a complementary perspective by explicitly incorporating the contact structure and the heterogeneity of individual interactions.

The model proposed in this paper builds on an established node-based mean-field methodology for diffusion processes on complex networks. Its main distinguishing feature is the explicit separation of spreading individuals into clients and nonclients of the advertised product. This distinction allows the dissemination of advertising information to be studied while retaining information about the customer status of the individuals participating in the spreading process.

The mathematical analysis characterizes the invasion thresholds of the network model and its homogeneous reduction. These thresholds describe the local growth or decay of small spreading perturbations around diffusion-free (or, more appropriately in this context, spreader-free) equilibria. In particular, the threshold conditions must not be interpreted as determining the final proportion of targets or inactive individuals. The system admits a family of spreader-free equilibria, and the final distribution between the target and inactive compartments depends on the initial conditions and the evolution of the diffusion process.

The numerical experiments illustrate the influence of model parameters, network topology, and the choice of initially spreading individuals on the propagation dynamics. Furthermore, the comparison with stochastic Monte Carlo simulations provides an assessment of the accuracy of the first-order mean-field approximation. The results show that this accuracy depends on the structural properties of the underlying network, with larger discrepancies observed in some sparse or highly clustered network configurations.

These observations emphasize that the deterministic equations should be interpreted as an approximation to the marginal dynamics of the underlying stochastic process rather than as an exact description of those dynamics.

An important direction for future research is the validation of the proposed framework using empirical diffusion data. Such validation would require temporal information on message propagation together with the underlying or reconstructed contact network. Observed sharing events could be used to identify spreading and nonspreading individuals and to estimate model parameters through statistical inference or numerical calibration. When customer/noncustomer information is available, for example, through campaign conversion data, purchase records, or complementary surveys, the two spreading compartments S_c and S_n could also be distinguished empirically. The calibrated model could then be evaluated by comparing its predictions with observations not used during parameter estimation. Relevant quantities include temporal diffusion patterns, overall campaign reach, and observed individual state transitions. We note, however, that distinguishing customers from non-customer spreaders represents an important practical challenge when only public social-network data are available.

Although the present work has been formulated in the context of viral marketing, the distinction

between adoption and information sharing makes the framework potentially applicable to other information-diffusion processes. In public health communication, for example, the target compartment could represent individuals who have not yet received a health message; spreading adopters could represent individuals who follow a recommended behavior and also disseminate the message; spreading nonadopters could represent individuals who disseminate the information without adopting the recommended behavior; and inactive individuals could represent informed individuals who no longer participate in its diffusion.

With an appropriate reinterpretation and calibration of the transition parameters, this framework could therefore be explored in vaccination-awareness, disease-prevention, or other public-health communication campaigns. Such applications would require domain-specific data and should be regarded as potential extensions of the present model rather than as validated applications at this stage.

Further research may also investigate higher-order moment closures, alternative network structures, and extensions incorporating additional behavioral mechanisms or time-dependent contact patterns.

Author contributions

A. Martin del Rey: Conceptualization of this study, Methodology, Writing – original draft. J.D. Hernandez Guillen: Software, Writing – review & editing.

Use of Generative-AI tools declaration

The authors declare that they used artificial intelligence (AI) tools, specifically ChatGPT, to proofread the English of this work in order to improve clarity, coherence, and overall writing quality.

Conflict of interest

A. Martin del Rey is an editorial board member for AIMS Mathematics and was not involved in the editorial review or the decision to publish this article. All authors declare that there are no competing interests.

References

1. M. T. Ewing, D. B. Stewart, D. R. Mather, J. D. Newton, How contagious is your viral marketing campaign? A mathematical model for assessing campaign performance, *J. Advert. Res.*, **54** (2014), 205–216. https://doi.org/10.2501/JAR-54-2-205-216
2. H. S. Rodrigues, M. J. Fonseca, Can information be spread as a virus? Viral marketing as epidemiological model, *Math. Methods Appl. Sci.*, **39** (2016), 4780–4786. https://doi.org/10.1002/mma.3783
3. J. Yang, D. Zhuang, W. Xie, G. Chen, A study of design approach of spreading schemes for viral marketing based on human dynamics, *Physica A*, **392** (2013), 6494–6505. https://doi.org/10.1016/j.physa.2013.07.059

4. J. Yang, C. Yao, W. Ma, G. Chen, A study of the spreading scheme for viral marketing based on a complex network model, *Physica A*, **389** (2010), 859–870. https://doi.org/10.1016/j.physa.2009.10.034
5. A. Tavasoli, H. Shakeri, E. Ardjmand, W. A. Young, Incentive rate determination in viral marketing, *Eur. J. Oper. Res.*, **289** (2021), 1169–1187. https://doi.org/10.1016/j.ejor.2020.07.046
6. Y. Ulyana, P. Andrij, Conceptual model the speed of information dissemination in social networks on the basis of the Monod equation, in *Proceedings of the 12th International Scientific and Technical Conference on Computer Sciences and Information Technologies (CSIT 2017)*, **1** (2017), 318–321. https://doi.org/10.1109/STC-CSIT.2017.8098795
7. J. N. C. Gonçalves, H. S. Rodrigues, M. T. Monteiro, A contribution of dynamical systems theory and epidemiological modeling to a viral marketing campaign, *Adv. Intell. Syst. Comput.*, **557** (2017), 974–983. https://doi.org/10.1007/978-3-319-53480-0_96
8. J. N. C. Goncalves, H. S. Rodrigues, M. T. Monteiro, Optimal control strategies for an advertisement viral diffusion, in *Operational Research*, A. I. F. Vaz, J. P. Almeida, J. F. Oliveira, A. A. Pinto (eds.), Springer Proceedings in Mathematics & Statistics, **223** (2018), 135–149. https://doi.org/10.1007/978-3-319-71583-4_10
9. S. Bhattacharya, K. Gaurav, S. Ghosh, Viral marketing on social networks: An epidemiological perspective, *Physica A*, **525** (2019), 478–490. https://doi.org/10.1016/j.physa.2019.03.008
10. K. J. Sharkey, Deterministic epidemiological models at the individual level, *J. Math. Biol.*, **57** (2008), 311–331. https://doi.org/10.1007/s00285-008-0161-7
11. P. Van Mieghem, J. Omic, R. Kooij, Virus spread in networks, *IEEE/ACM Trans. Netw.*, **17** (2009), 1–14. https://doi.org/10.1109/TNET.2008.925623
12. R. Pastor-Satorras, C. Castellano, P. Van Mieghem, A. Vespignani, Epidemic processes in complex networks, *Rev. Mod. Phys.*, **87** (2015), 925–979. https://doi.org/10.1103/RevModPhys.87.925
13. D. J. Daley, D. G. Kendall, Epidemics and rumours, *Nature*, **204** (1964), 1118. https://doi.org/10.1038/2041118a0



AIMS Press

© 2026 the Author(s), licensee AIMS Press. This is an open access article distributed under the terms of the Creative Commons Attribution License (https://creativecommons.org/licenses/by/4.0)